Li *et al. Energy Mater.* **2025**, *5*, 500005
DOI: 10.20517/energymater.2024.31

Energy Materials

Review

Open Access

Check for updates

Multifunctional MXene inks for printed electrochemical energy storage devices

Zhuo Li[1], Qinglong He[1], Hao Chen[1], Yiwen Chen[1], Chuijin Zeng[1], Tianyue Xu[1], Shungui Deng[1,2,3], Chuanfang Zhang[1,*]

[1]College of Materials Science & Engineering, Sichuan University, Chengdu 610065, Sichuan, China.
[2]Laboratory for Functional Polymers, Swiss Federal Laboratories for Materials Science and Technology (EMPA), Dübendorf CH-8600, Switzerland.
[3]Institute of Materials Science and Engineering, Ecole Polytechnique Federale de Lausanne (EPFL), Lausanne CH-1015, Switzerland.

***Correspondence to:** Prof. Chuanfang Zhang, College of Materials Science & Engineering, Sichuan University, South Section 1, Rd. #24, Yihuan Road, Chengdu 610065, Sichuan, China. E-mail: chuanfang.zhang@scu.edu.cn

How to cite this article: Li, Z.; He, Q.; Chen, H.; Chen, Y.; Zeng, C.; Xu, T.; Deng, S.; Zhang, C. Multifunctional MXene inks for printed electrochemical energy storage devices. *Energy Mater.* **2025**, *5*, 500005. https://dx.doi.org/10.20517/energymater.2024.31

Received: 18 Apr 2024 **First Decision:** 6 Jun 2024 **Revised:** 27 Jun 2024 **Accepted:** 24 Jul 2024 **Published:** 6 Jan 2025

Academic Editors: Hao Liu, Giovanni B. Appetecchi **Copy Editor:** Fangling Lan **Production Editor:** Fangling Lan

Abstract

Since the discovery of MXenes, the family has expanded rapidly in the past decade. With their fascinating properties, including high electrical conductivity, solution processability, tunable surface functionality, and excellent mechanical properties, MXenes have garnered significant enthusiasm from the academic community and industrial relevance. The most extensively studied of the many applications for MXene-based devices is electrochemical energy storage (EES). Importantly, MXene inks allow quick yet efficient production of personal EES devices through additive manufacturing. However, there are relatively few comprehensive summaries of reports on the processing of MXene inks for EES devices. This paper provides a comprehensive review of MXene synthesis, additive manufacturing strategies and the latest advancements in the printing of MXene-based high-performance EES devices including micro-supercapacitors and batteries. Besides, the current challenges for high precision and high-performance printing technology are also discussed. This review is expected to provide valuable insights for solution processing of MXene inks and may shed light on the large-scale application of MXenes toward the next generation of wearable electronics.

Keywords: Functional inks, MXenes, solution processing, energy storage devices, wearable electronics

© The Author(s) 2025. **Open Access** This article is licensed under a Creative Commons Attribution 4.0 International License (https://creativecommons.org/licenses/by/4.0/), which permits unrestricted use, sharing, adaptation, distribution and reproduction in any medium or format, for any purpose, even commercially, as long as you give appropriate credit to the original author(s) and the source, provide a link to the Creative Commons license, and indicate if changes were made.

INTRODUCTION

With the rapid development of wearable and portable smart electronic devices, there is a growing demand for high-performance electrochemical energy storage (EES) devices[1-7], especially for rechargeable batteries[8,9] and supercapacitors (SCs)[10,11]. Rechargeable batteries are able to store more charge due to the redox reactions occurring in the electrode-electrolyte interface, thus possessing a much higher energy density compared to that of SCs, but their lower power densities restrict their suitability for high-power applications and fast charging. In contrast, SCs can be charged in seconds and provide higher power densities. To achieve high-performance EES devices (EESDs), numerous efforts have been devoted to investigating electrode materials with large specific surface area (SSA), high electrochemical activity, and fast charge transport[12-14].

Owing to the exceptional physical and chemical properties, along with the unique structural characteristics including atomic-level thickness, which provide more exposed surface area and better ion transport, two-dimensional (2D) materials have recently gained attention of researchers as prospective options for energy storage[15-18]. After the discovery of graphene, different classes of 2D materials, including transition metal dichalcogenides (TMDs)[19,20], silicene[21,22], layered double hydroxides (LDHs)[23,24], phosphorene[25,26], and MXenes[27,28] have been successively developed. As a novel 2D material, MXenes are a novel class of transition metal carbides, nitrides, and carbonitrides[29]. Discovered in 2011[30], MXenes have the general formula $M_{n+1}X_nT_x$ (n = 1,2,3 or 4), where M represents an early transition metal, X stands for C and/or N, and T_x refers to various functional groups such as -OH, -O, -F. The surface functional groups endow a good hydrophilicity while the metallic backbone provides excellent electrical conductivity. MXenes have excellent electrochemical, electronic, optical, and mechanical properties and show promising applications in various fields, such as energy storage[31], sensors[32], optoelectronics[33], electronics[34], biomedicine[35], and catalysis[36]. The predominant strategy for large-scale preparation of 2D material nanosheets is intercalation exfoliation due to low cost, solution processability and high yield of monolayers[37].

When the exfoliation flakes are redispersed in solvents and assisted by additives, printable 2D materials inks can be formulated, allowing EESDs to be fabricated using simple, efficient and scalable printing technologies. Compared to traditional manufacturing techniques, the simplicity, low cost and high efficiency of printing technology, as well as its scalability, demonstrate significant potential for manufacturing energy storage devices. The first thing to consider when printing EESDs is the appropriate printing technology. Different printing technologies vary in terms of resolution, printing speed, film thickness, and so on. The appropriate printing technology should be selected for different application requirements. Inks with specific rheological requirements should be formulated for different printing technologies to ensure smooth printing. In order to meet the rheological requirements, the ink additives, such as binders, surfactants, and rheology modifiers, are typically employed to promote the deposition and molding of materials. However, the subsequent high-temperature heat treatment to remove additives leads to the degradation of material properties and the complexity of the manufacturing process. In addition, the thermal annealing treatment also limits the choice of soft substrates, including plastics, polymers, plant leaves, or even human skin. The 2D materials inks, such as graphene[38], molybdenum disulfide[39], black phosphorus[40], and MXene inks[41,42], can be printed on different substrates using various printing methods and show good performance.

Printable MXene inks for EESDs (mainly MSCs and batteries) have received a lot of attention due to the excellent rheological, conductive and mechanical properties of MXenes[43,44]. The unique surface chemistry of MXenes allows them to be stably dispersed in both aqueous and polar solvents and to be formulated directly into inks without additives, which is the prerequisite of additive manufacturing of various

functional devices using diverse printing technologies, such as inkjet printing[45,46], screen printing[47,48], three-dimensional (3D) printing[49,50], *etc.* [Figure 1]. However, printable MXene inks still present certain challenges that researchers are striving to address. The research group is currently focusing on improving the stability of MXene inks and achieving scale production. MXene oxidizes easily in humid environments, which compromises the structural integrity of the nanosheets and thus reduces the performance of MXene inks. Consequently, improving the oxidation stability of MXene inks is an approach for realizing high-performance MXene-based printed devices. To accomplish the large-scale production of MXene inks, a few areas of research need to be explored, involving the synthesis methods of MXenes, the rheology of inks, and printing processes. The performance of the fabricated EESDs depends mainly on the quality of the print. Thus, ink formulation is crucial to improving print quality and involves scalable production of high quality MXene, ink formulation and printing techniques. Besides, the research and application of non-titanium-based MXene materials with outstanding properties is still relatively limited and needs further exploration[28].

This review summarizes recent advancements in MXene-based printed energy storage devices and flexible electronics. First, various strategies for MXene ink formulation are briefly discussed. Next, the advantages and limitations of different printing technologies are presented. Besides, multiple applications of MXene-based printing technologies, such as batteries, SCs, and flexible electronics, are exemplified. Finally, the paper concludes the main challenges and lists the opportunities for MXene-based printing technologies.

SYNTHESIS METHODS OF MXENE AND INK FORMULATION

Bottom-up strategy to synthesize MXenes

Distinct synthesis methods affect the quality and properties of subsequent MXene. Bottom-up synthesis methods have proven to be a versatile strategy for the synthesis of high-quality 2D materials with large areas. This strategy makes it possible to directly grow ultrathin 2D crystals while bypassing the precursor, extending the possibilities for more intriguing applications. Currently, the bottom-up strategy is mainly based on chemical vapor deposition (CVD), which has the advantage of efficiently synthesizing MXene with unique surface chemistry and high yield[62,63] [Figure 2A]. For example, Wang *et al.* developed the direct synthesis of Ti_2CCl_2 flowers supported on Ti foil by choosing $TiCl_4$ and graphite as the Ti and C sources, respectively, and heated up at 950 C[64]. They also demonstrated the synthesis of Ti_2N using this strategy [Figure 2B]. Besides, Xiang *et al.* chose gaseous $TiCl_3$ and CH_4 as the Ti and C sources, respectively[65]. The reaction temperature is lower (850 C); the product Ti_2CCl_2 is highly crystalline with a much higher yield, which can be produced in kg in a single batch. Moreover, when dispersing Ti_2CCl_2 in water, a homogeneous solution is thus formed without the necessity of any surfactant, similar to conventional MXene flakes. The gas-phase assembled Ti_2CCl_2 film also possesses a higher electrical conductivity and much longer shelf life than conventional Ti_2CT_x films and solutions, demonstrating the unique advantage of their methodology. Over the past decade, the top-down strategy has been studied extensively by researchers. Since the first reported MXene in 2011, many methods of selective etching have been developed, including hydrofluoric acid (HF) etching[66], *in-situ* formed HF etching[67], alkali etching[68], and molten salt etching[69], electrochemical etching[70], and so on. We therefore briefly review several different classical methods of selective etching.

Top-down strategy to synthesize MXenes

Since the successful etching of the Al layer from Ti_3AlC_2 to obtain MXene in 2011, the top-down strategy has been the main preparation strategy for MXene, consisting of two stages: selective etching and delamination [Figure 2C][71].

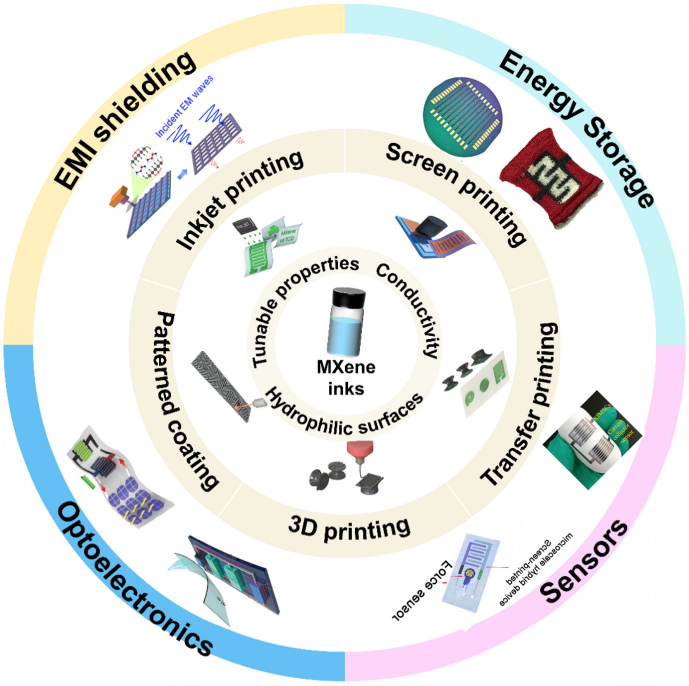

Figure 1. Various printing and coating technologies and applications of MXene for printed electronics. The technologies including inkjet printing, screen printing, transfer printing, 3D printing, patterned coating, *etc.* Reproduced with permission[51]. Copyright 2018, John Wiley and Sons. Reproduced under terms of the CC-BY license[52]. Copyright 2019, Springer Nature. Reproduced with permission[53]. Copyright 2020, John Wiley and Sons. Reproduced with permission[54]. Copyright 2019, John Wiley and Sons. The applications including sensors, optoelectronics, energy storage and EMI shielding. Sensors: Reproduced with permission[55]. Copyright 2018, Elsevier. Reproduced with permission[56]. Copyright 2021, John Wiley and Sons. Optoelectronics: Reproduced with permission[57]. Copyright 2021, John Wiley and Sons. Reproduced with permission[58]. Copyright 2021, John Wiley and Sons. Energy storage: Reproduced with permission[59]. Copyright 2020, Elsevier. Reproduced with permission[60]. Copyright 2019, John Wiley and Sons. EMI shielding: Reproduced with permission[61]. Copyright 2021, Elsevier.

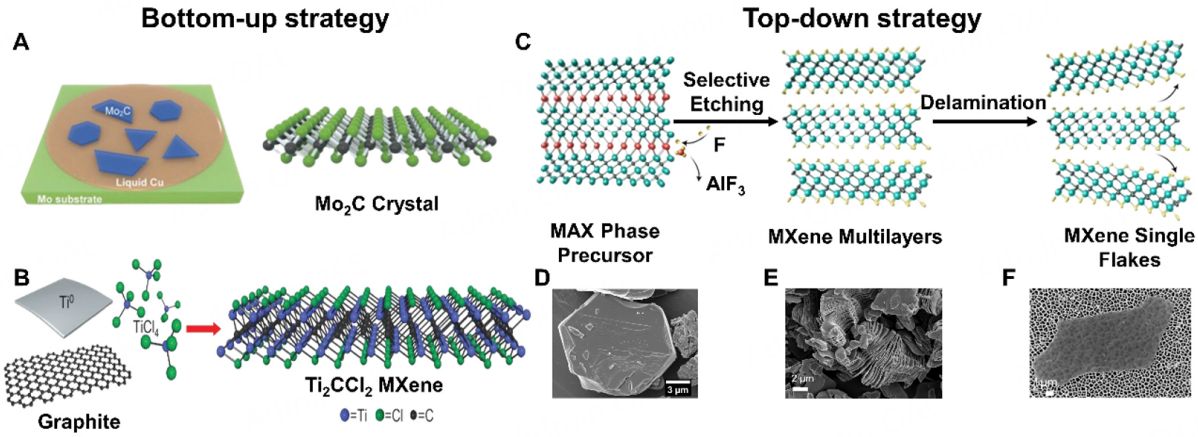

Figure 2. Synthesis of MXenes by bottom-up and top-down strategies. Schematic of 2D Mo_2C (A) and Ti_2CCl_2 (B) produced by CVD method. (C) Schematic illustration of the synthesis process by top-down strategy. Scanning electron microscope (SEM) image of Ti_3AlC_2 MAX phase (D) and $Ti_3C_2T_x$ multilayers (E) $Ti_3C_2T_x$ MXene flakes (F). Reproduced with permission[62]. Copyright 2017, John Wiley and Sons. Reproduced with permission[64]. Copyright 2023, American Association for the Advancement of Science. Reproduced with permission[71]. Copyright 2022, Springer Nature. Reproduced with permission[73]. Copyright 2021, American Chemical Society. Reproduced with permission[82]. Copyright 2017, American Chemical Society.

Selective etching

The MAX phase serves as the MXene precursor and typically refers to a class of ternary layered compounds with a formula of $M_{n+1}AX_n$, where M is an early transition metal (e.g., Sc, Ti, V, Cr, Zr), A represents a group III A or IV A element (Al, Ga), and X is C and/or N[72,73] [Figure 2D]. Selectively etching the A element in the MAX phase yields MXene with alternating M and X elements. Currently, there are four known main structures of MXene: M_2X, M_3X_2, M_4X_3 and M_5X_4. Similar to the MAX phase, MXene has a hexagonal close packing crystal structure with $P6_3/mmc$ space group symmetry, with M atoms in a close packing arrangement and X atoms in the octahedral gap[74].

Selective etching of the MAX phase is the first step to obtain monolayered or few-layered MXenes. In the MAX phase, the M-X bonds are covalent and chemically strong, while the M-A bonds are metallic, with weaker bonding energy and stronger chemical activity[75]. Therefore, it is difficult to obtain MXene directly by the mechanical exfoliation method used for graphene preparation. Instead, chemical etching should be used to prepare MXene by preferentially breaking the M-A bond while retaining the M-X bond, taking advantage of the weaker chemical bonding energy of M-A compared to M-X. The etching conditions are associated with the MAX phase and rely on factors such as M-A atomic binding strength, particle size, and crystal structure[31].

Since Naguib *et al.* first employed HF selective etching route at room temperature (RT) to prepare $Ti_3C_2T_x$, etching the MAX phase with HF has become the most widely used method to produce MXene with an accordion-like morphology[30]. However, this method relies heavily on hazardous HF solutions. Ghidiu *et al.* reported the use of a mixture of HCl and LiF as an alternative etchant instead of HF, which generates HF *in-situ* and selectively etches the A atomic layer away[76]. This alternative method is simpler, safer, and faster, as LiF and HCl are much milder than HF etchants. However, this method still involves HF. The synthesis of MXene without HF has generated interest among researchers. Li *et al.* showed the synthesis of fluorine-free high-purity MXene using alkali etching (27.5 M NaOH, 270 C), providing a novel idea for the safe and green synthesis of MXene[77]. Pang *et al.* reported a simple and safe electrochemical etching method using dilute hydrochloric acid for the fast and gentle preparation of Ti_2CT_x, which was successfully extended to V_2C and Cr_2C, providing another idea for HF-free synthesis of MXene[70]. Li *et al.* reported the synthesis of Cl-terminated MXene ($Ti_3C_2Cl_2$ and Ti_2CCl_2) using Lewis molten salt via redox A-sites of MAX to achieve structural transformation[78], and varying the anion in molten salt results in different halogenated MXenes ($Ti_3C_2Br_2$ and $Ti_3C_2I_2$)[79]. By further extending the Lewis molten salt and the precursor MAX species, a generalized method for the synthesis of MXene by etching the MAX phase with Lewis molten salts has been reported. This provides another safe and scalable method for the fluorine-free synthesis of MXene[69].

Intercalation and delamination strategies

Therefore, weakening the interaction force between MXene layers is crucial to effectively delaminate multilayer MXene[80]. After selective etching, the multilayered (m-) MXene surface is terminated by hydrophilic, electronegative functional groups, mainly -F, -OH, -O, *etc.* [Figure 2E][81]. Strong forces between the multilayer MXene layers and the incomplete etching process lead to delamination difficulties. Through intercalating molecules and ions into stacked MXene layers to enlarge the interlayer spacing and weaken the interlayer interaction, the ultrasonication or manual handshaking is able to delaminate the swollen solids into predominantly single-layer MXene flakes [Figure 2F][82]. Organic intercalating agents, such as polar organic molecules (e.g., dimethyl sulfoxide (DMSO)[83], urea[84], hydrazine[85]), and other large organic alkali molecules[86] [e.g., tetrabutylammonium hydroxide (TBAOH) or tetramethylammonium hydroxide (TMAOH)], have been effectively employed. In the early stages of the study, researchers had already reported that chemical intercalation using DMSO successfully enlarged the layer spacing (~15.4 Å), followed by simple sonication to obtain a single layer of MXene. m-MXene can also be intercalated by alkali

metal ions[87], such as Li^+, Na^+, K^+, and Mg^{2+} to swell the solids.

Following the swelling the m-MXene, delamination is the crucial step to realize single-or-few-layered MXene dispersions, which is the prerequisite of forming aqueous inks. The easiest way to delaminate the swollen MXene solids is through ultrasonication, whose condition determines the quality of MXene flakes (concentration, flake size, pin-holes, defects quantity and density, *etc*.[88]). For instance, longer time and higher power ultrasonication produces MXene flakes with many defects and reduces the lateral size. Therefore, it is essential to develop delamination methods that do not require ultrasonic treatment. For instance, Shahzad *et al*. developed the minimally intensive layer delamination (MILD) method, which produces large clean flakes with fewer defects by manual shaking instead of ultrasonic treatment[89]. This method used mixed lithium fluoride and hydrochloric acid to achieve etching and intercalation at the same time in which hydrated lithium ions intercalate into the interlayer, significantly increasing the interlayer spacing. Currently, this method has become the main route to prepare high quality MXene with large flakes. Top-down methods are more suitable for scale production than bottom-up strategies. However, their etching process and subsequent delamination can cause the MXene to become smaller and introduce defects. In addition, the choice of MAX precursors limits the types and structures of the prepared MXene.

MXene inks formulation and rheological properties

In general, inks are composed of three parts: active materials, solvents and additives. The active material is the main component of the ink, such as the 2D materials graphene, molybdenum disulfide, MXene, and so on. Solvents are divided into two categories: aqueous and organic. The selection of solvents depends on the solute-solvent interactions; only those possessing surface tension similar to that of the solute result in good dispersions. In addition, the solvents should showcase a certain degree of volatility such that the ink drying kinetics is fast enough without interrupting the printing process. Additives include binders, surfactants and rheology modifiers. Although the use of additives greatly improves the rheological properties of the ink, thereby improving processability, the additive removal treatments require high temperatures, which not only reduce the performance of the ink, but also complicate the whole process.

MXene inks are suspensions or dispersions containing MXene flakes with different rheological properties that can be deposited using printing or coating techniques. Different printing technologies have distinct rheological requirements for MXene inks. Figure 3A illustrates the relationship between viscosity, throughput, resolution, film thickness and transparency with multiple printing technologies. The rheological behavior of MXene inks is mainly described by their viscosity. Viscosity can be measured as the ratio of shear stress to shear rate. MXene inks are pseudoplastic fluids with a shear thinning behavior; the viscosity decreases with the increase in the shear stress. The shear thinning behavior ensures the smooth flow of the ink through the nozzle without clogging, enabling the deposition on the substrate. The viscosity of MXene inks is related to a number of factors[90], including MXene ink concentration, MXene flake size distribution, solvents, *etc*., with the concentration of the dispersion being the main parameter.

Various concentrations of MXene inks exhibit distinct rheological behaviors [Figure 3B]. For example, for aqueous monolayer $Ti_3C_2T_x$ dispersions, as each order of magnitude increase in MXene concentration, the viscosity increased with it by three orders of magnitude (at low shear rate)[91]. The viscosity of MXene inks can be controlled by modulating the size and the thickness of the MXene laminates. The study of two aqueous inks with two different MXene flake sizes, denoted as L-$Ti_3C_2T_x$ ink (average size 2 μm), and S-$Ti_3C_2T_x$ ink (average size 350 nm), showed that at similar concentrations (18 mg mL^{-1} of L- $Ti_3C_2T_x$ ink *vs*. 18.8 mg mL^{-1} of S-$Ti_3C_2T_x$ inks), the viscosity of L-$Ti_3C_2T_x$ ink (5.1 cP) was significantly higher than that of S-$Ti_3C_2T_x$ ink (≈1.5 cP)[92].

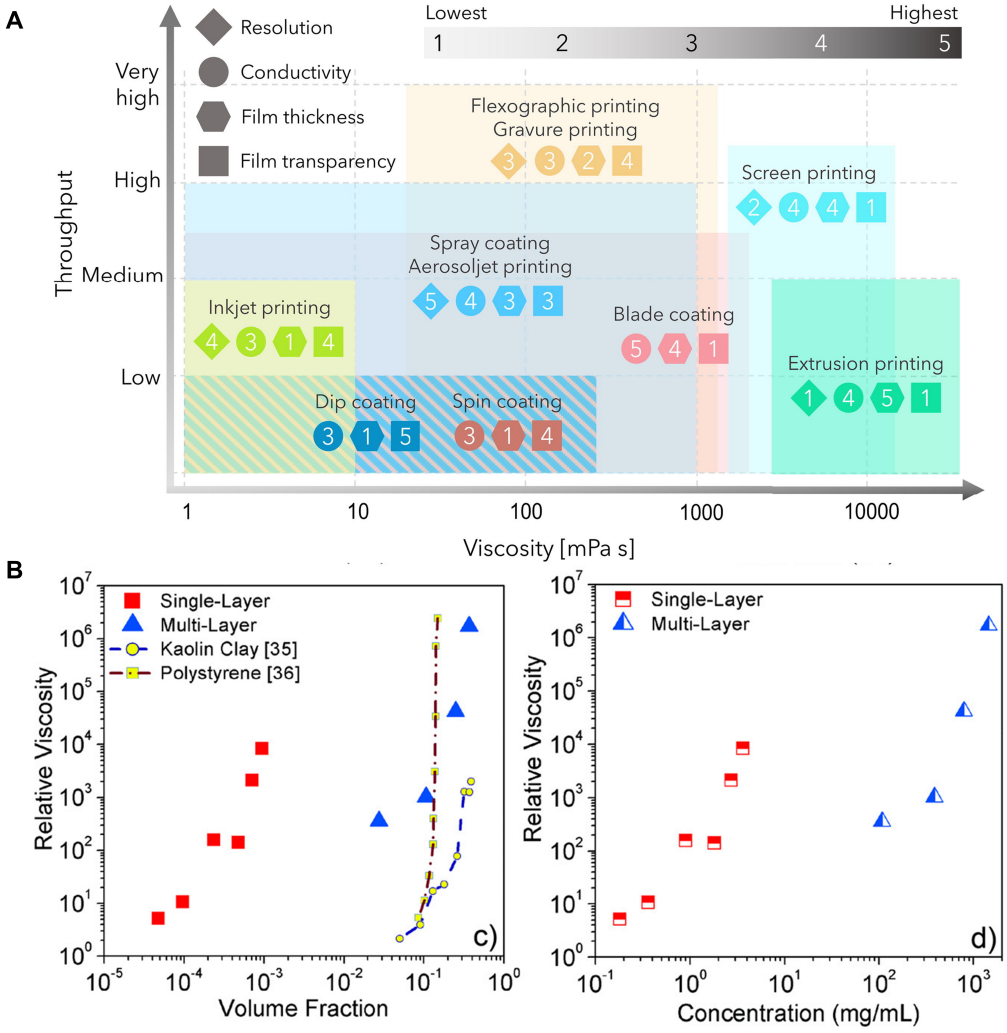

Figure 3. Rheological properties of MXene inks. (A) Relationship between viscosity, yield, resolution, film thickness and transparency with different printing technologies. Reproduced with permission[54]. Copyright 2021, Elsevier. (B) Plots of relative viscosity *vs.* volume fraction and measured viscosity *vs.* concentration for single and multilayer $Ti_3C_2T_x$ dispersions. Reproduced with permission[91]. Copyright 2018, American Chemical Society.

In addition, MXene inks dispersed in varying solvents showcase differing rheological behaviors. Water is the most common dispersing medium because MXene has surface hydrophilic functional groups that allow stable dispersion in water or hydrophilic media[93]. For organic solvents, solvents with a surface tension that better matches that of the MXene are more stable in dispersion. Common good solvents are DMSO, N,N-dimethylformamide (DMF), N-methyl-2-pyrrolidone (NMP), *etc.*[83]. In addition, the ink should have good wettability, implying continuous contact between the ink and the substrate for the integrity of the printed pattern. Wettability can be determined by the contact angle between the ink droplets and the substrate. According to Young's equation, when the contact angle is greater than 90, the wettability is poor, which, in turn, leads to poor ink printing, while when the contact angle is less than 90, the situation is completely opposite. In order to improve the wettability, the key is to choose a suitable solvent to adjust the surface tension of the ink, so that it matches the surface energy of the substrate[94]. The surface tension of the ink should be 7-10 mN m^{-1} lower than the surface energy of the substrate[95]. Compared to dispersion in an aqueous medium, the use of organic solvents as a dispersion medium slows down the degradation of

MXene. Based on the formulated MXene inks with good rheological properties, which are well matched to the printing technologies, various patterns and functional devices, including EESDs, can be quickly obtained through direct printing.

MXene-based MSCs

Micro-SCs (MSCs) have received great attention owing to their high-power density, long cycle life, fast charging speed and small area[96-98]. At present, the common MSC structure is a planar interdigital structure with two adjacent electrodes placed separately. The narrow gap between the interdigital electrodes shortens the ion diffusion distance, thus accelerating the ion transport kinetics which correspondes to higher charge/discharge rates in the MSC devices. The areal capacitance is commonly used as an indicator to evaluate the performance of MSCs. Currently, efficient fabrication strategies for fabricating MSCs include but are not limited to photolithography[99], laser scribing[100] and printing technology[101]. The complex and time-cost fabrication process of photolithography and the selection of active materials for laser scribing have limited its development. Printing technology is an additive manufacturing technology that has gained increased attention due to its simplicity, low cost, and scalability, allowing for the manufacturing of devices on a large scale[102]. Printing technologies can be classified as digital and non-digital categories based on whether a template is utilized during the printing process. Inkjet and 3D printing are examples of digital printing, while screen and transfer printing fall under non-digital printing. Each printing technique requires specific fluidic properties and the ink rheology. The advantages and limitations in the application of different printing technologies are summarized in Table 1. It is noteworthy that the printed MSCs are typically operated at a voltage below 0.6 V owing to the unique properties of MXene. Its narrow voltage window greatly limits the energy density of the MSCs. This limitation can be mitigated by optimizing the electrolyte and designing asymmetric MSCs. In the following paragraphs, we focus on the MXene MSCs achieved via different printing techniques. Table 2 is a summary of the reported printed/coated MSCs.

Inkjet printing

Inkjet printing is a widely used digital, high-resolution, non-contact printing technology that is employed in the manufacturing of various devices, including energy storage[118] and optoelectronic devices[119]. This method is able to produce miniatured devices with much reduced dimensions while demonstrating a high integrity substrate/geometry compatibility and scalability. The 2D materials such as graphene[120] and MoS_2 nanosheets[121] have been formulated into functional inks for inkjet printing. The quality of the inkjet-printed patterns depends on three factors: the substrate, ink rheology, and printing parameters. In addition, ink parameters such as Reynolds number (Re), Ohnesorge number (Oh), and Weber number (We) are frequently used to evaluate the ink printability. By calculating the inverse Ohnesorge number based on the following equation, Z of the ink, researchers can better understand the ink's properties[122]. The Z value depends on surface tension (γ), density (ρ), diameter of the jetting nozzle (a), and viscosity (η), respectively.

$$Z = \frac{1}{Oh} = \frac{Re}{\sqrt{We}} = \frac{\sqrt{\gamma \rho a}}{\eta} \tag{1}$$

$$Re = \frac{v \rho a}{\eta} \tag{2}$$

$$We = \frac{v^2 \rho a}{\gamma} \tag{3}$$

To form stable droplets, the Z value should be between 1 and 14[123]. For water-based inks, the high surface tension of water results in a Z value higher than 14. According to the equation, it is necessary to increase the viscosity appropriately to reduce the Z value [Figure 4A]. The maximum viscosity value depends on the diameter of the jetting nozzle that allows the ink to pass through the printer without clogging. Uzun *et al.* prepared aqueous, additive-free MXene inks with different concentrations and flake sizes to modify the

Table 1. Summary of the advantages and disadvantages of different printing technologies

Printing methods	Advantages	Disadvantages
Inkjet printing	Less material required Environmentally friendly Low-cost	Nozzle clogging
Screen printing	High-speed production Low waste	Low resolution High roughness
Transfer printing	Small wastage	High volume inks Extra step
Direct ink writing	Scalable	Low resolution

Table 2. Summary of printed MXene-based MSCs

Ref	Materials	Printing/coating methods	Electrolyte	Electrochemical performance
[103]	SA-$Ti_3C_2T_x$	Inkjet printing	PVA/H_2SO_4	108.1 mF cm^{-2}
[104]	$Ti_3C_2T_x$/graphene	Inkjet printing	PVA/Na_2SO_4	3.84 mF cm^{-2}
[105]	$Ti_3C_2T_x$-N	Screen printing extrusion printing	H_2SO_4	70.1 mF cm^{-2} 8.2 F cm^{-2}
[106]	$Ti_3C_2T_x$/CNF	3D printing	H_2SO_4	2.02 F cm^{-2}
[107]	$Ti_3C_2T_x$	3D printing	PVA/H_2SO_4	2.337 F cm^{-2}
[108]	$Ti_3C_2T_x$/MnO_2	Inkjet printing	PVA/Na_2SO_4	0.51 μWh cm^{-2}
[109]	NiS/N-$Ti_3C_2T_x$	Inkjet printing	PVA/KOH	33.5 mWh cm^{-3}
[52]	$Ti_3C_2T_x$	Inkjet printing extrusion printing	PVA/H_2SO_4	562 F cm^{-3}
[110]	$Ti_3C_2T_x$@C	Inkjet printing	PVA/H_2SO_4	40 mF cm^{-2}
[111]	$Ti_3C_2T_x$	3D printing	PVA/H_2SO_4	1,035 mF cm^{-2}
[112]	V_2CT_x	Direct ink writing	PVA/Zn $(CF_3SO_3)_2$	3.82 F cm^{-2}
[113]	$Ti_3C_2T_x$	Inkjet printing	PVA/H_3PO_4	192 μF cm^{-2}
[114]	Ag@Ti_3C_2 MnO_2@Ti_3C_2	Direct ink writing	KOH	38.16 Wh kg^{-1}
[51]	$Ti_3C_2T_x$	Stamping	PVA/H_2SO_4	61 mF cm^{-2}
[115]	$Ti_3C_2T_x$	Blade coating	PVA/H_2SO_4	241 mF cm^{-2}
[116]	MX/CCNS	Vacuum filtration Screen printing	PVA/H_2SO_4	114.9 mF cm^{-2}
[117]	$Ti_3C_2T_x$/PH1000	Vacuum filtration	H_2SO_4	23 mWh cm^{-3}

viscosity [Figure 4B][92]. Two types of MXene inks with calculated Z values of 19.9 and 18.9 were able to form stable droplets. A symmetrical MSC with planar interdigitated structure was fabricated by inkjet printing on a cotton substrate, and the effects of flake sizes and the number of printed paths on MSC performance were investigated. The resistance of the printed pattern of the L-$Ti_3C_2T_X$ ink (micrometer scale) is lower than the S-$Ti_3C_2T_X$ ink (sub-micrometer scale) because of the reduced intersheet contact area for the L-$Ti_3C_2T_X$ ink. Furthermore, the resistance of L-$Ti_3C_2T_X$ and S-$Ti_3C_2T_X$ inks decreases as the number of printed paths and the amount of active material increase. The specific areal capacitance of the MSCs printed with a mixture of the two inks was 60 and 32 mF cm^{-2} at 2 and 20 mV s^{-1}, respectively, which outperforms the rest of MSCs fabricated using other MXene inks. In addition, Zhang *et al.* prepared organic MXene inks without additives using a solvent-transfer strategy with Z values ranging from 1 to 14[52]. AlO_x-coated polyethylene terephthalate (PET) substrates were selected to ensure complete wetting of the organic ink with the substrate, resulting in high-resolution inkjet-printed patterns [Figure 4C]. By optimizing the number of printed paths and line gaps, the inkjet-printed MSCs using NMP inks demonstrated superior volumetric capacitance compared to other printed MSCs.

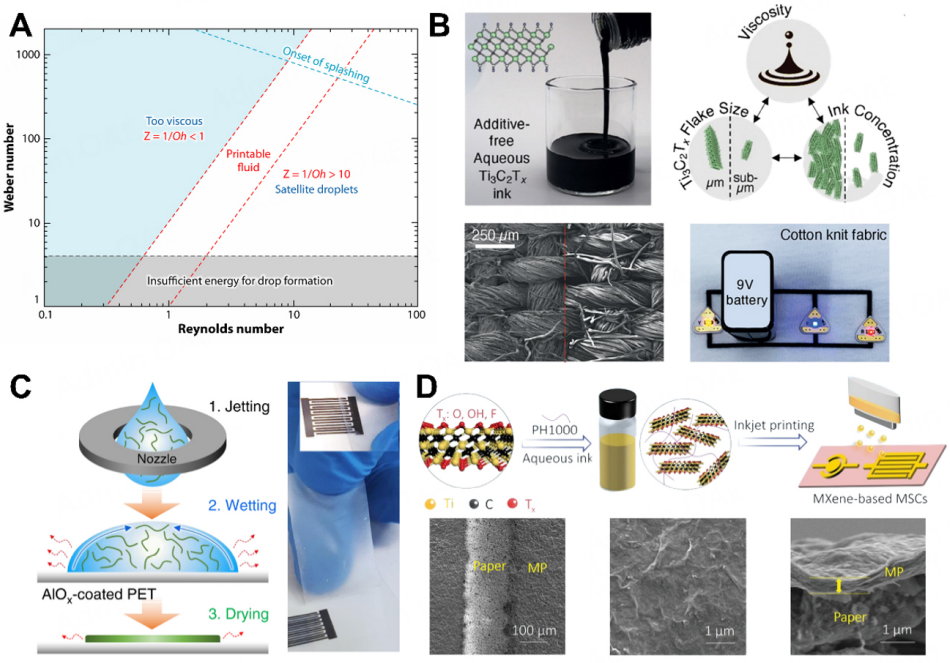

Figure 4. Inkjet printing of MXenes. (A) *Z*-value range for stable inkjet printing. Reproduced with permission[123]. Copyright 2010, Annual Reviews. (B) Key factors for additive-free $Ti_3C_2T_x$ ink formulation: ink concentration, flake size and viscosity, and SEM image of printing ink onto fabric surface. Reproduced with permission[92]. Copyright 2020, Wiley-VCH. (C) Diagram of inkjet printing using MXene organic ink and the corresponding high printing resolution patterns. The process consists of three steps: jetting, wetting, and drying. Reproduced under terms of the CC-BY license[52]. Copyright 2019, Springer Nature (D) Schematic of the inkjet printing MP-MSCs and SEM and Cross-sectional image of MP-MSC. Reproduced with permission[124]. Copyright 2021, Wiley-VCH.

However, the stacking of layered MXene makes ion diffusion difficult and reduces electrochemical performance. To address this issue, Ma *et al.* reported a hybrid ink of MXene/PH1000 to fabricate MSCs[124]. The highly conductive and water-soluble PH1000 was attached to the surface of the MXene sheets, effectively relieving the stacking of the MXene and facilitating ion transfer. In addition to inkjet-printed MSCs, a temperature sensor was also printed, based on which flexible, self-powered integrated systems were realized by connecting MSCs and the temperature sensor in series with a silicon film solar cell [Figure 4D].

Indeed, the practical application of MXene inks is hindered by the MXene stability issue. When MXene inks are exposed to humid environments, the edge oxidation of MXene begins, generating TiO_2 and reducing device performance[125]. To enhance the MXene ink stability, a feasible strategy is to protect the edges by capping. For instance, formulating sodium ascorbate (SA)-capped MXene inks (with Triton X-100 and propylene glycol as a modifier) significantly enhances the stability of printed electrodes[103]. In a related study, Sangili *et al.* prepared MXene@C using a hydrothermal method to inhibit the oxidation of Ti by H_2O and O_2, and the resulting ink exhibited long-term stability[110].

Screen printing

Screen printing involves transferring a template design onto a flat substrate using a mesh screen made of silk or nylon[126]. The process is simple, low-cost, highly productive, and highly scalable. This requires that the rheological properties of inks meet the high requirements of the printing process. In particular, the ink must remain in a liquid state on the screen for a long time, and dry quickly on the substrate to ensure that the printed pattern is clear and well-defined.

The rheological behavior of ink under high shear stress (> 500 Pa) is mainly influenced by the loss modulus G″ (G″ > G′), which governs the ink in the form of liquid. This ensures that the ink flows easily through the screen mesh onto the substrate during printing, resulting in a well-defined printed pattern. At lower shear stresses (< 100 Pa), the storage modulus G (G′ > G″) becomes the main influencing factor, causing the ink to behave like a solid and facilitating the solidification of the ink during printing. The viscosity of inks used for screen printing generally ranges between 2-50 Pa·s[127]. Although screen printing has the advantage of low cost and scalable printing capability, its resolution is relatively low (hundreds of μm). Therefore, screen printing is unsuitable for applications that require precise control of the film at nanometer size.

The main challenge in screen-printed MXene MSCs is the low areal capacitance. This is due to the low solid loading of MXene inks that meet the rheological requirements for screen printing, as well as the severe nanosheet restacking issue which greatly suppresses the ion diffusion process. There are three main strategies to improve the electrochemical properties: (1) increasing the ink concentration; (2) surface functionalization; and (3) incorporating spacers to prevent sheet stacking.

For instance, Abdolhosseinzadeh *et al.* reported the formulation of highly concentrated MXene sediments inks for screen printing of MSCs[128]. Delaminated-MXene (d-MXene) can be used as a conductive binder, by adding a little to the sediments, those unetched MAX and unexfoliated m-MXene solids through the formation of hydrogen bonds and van der Waals force between MXenes, resulting in a mass loading of 22 wt% in the sediment inks. The screen-printed MSCs exhibited excellent electrochemical properties with an area capacitance and energy density of 158 mF cm^{-2} and 1.64 μWh cm^{-2}, respectively. This innovation approach not only enhances the performance of MSCs but also transforms wasted MXene sediments into a valuable resource, reducing the cost of device fabrication for next-generation wearable smart electronic products [Figure 5A]. Furthermore, surface functionalization of MXene is another approach to improve the electrochemical performance of MSCs. Nitrogen-doped MXene (MXene-N) inks with uniform nitrogen doping and a porous structure have been reported for screen-printed MSCs[105]. The MXene-N inks were prepared using the template-guided method with the melamine-formaldehyde. Nitrogen doping in the MXene lattice enhances both electrical conductivity and electrochemical reactivity. MXene-N inks with varying viscosities were tuned for screen printing of MSCs. MSCs fabricated using screen-printing technology yielded a surface capacitance of 70.1 mF cm^{-2} [Figure 5B].

It is also believed that incorporating spacers prevents the sheet stacking and improves the electrochemical performance of the MSCs. Adjusting the material composition to prepare printed MXene nanocomposite inks can effectively enhance the electrochemical performance of the devices[129]. For instance, Li *et al.* developed a simple *in situ* method to produce RuO_2-xH_2O@MXene nanocomposites that can be combined with silver nanowires (AgNWs) as composite inks for high-performance, fully printed MSCs[130]. The RuO_2 nanoparticles in the nanocomposite possess a high pseudocapacitance while acting as spacers to prevent the self-restacking of MXene nanosheets, providing an effective network for ion diffusion. Meanwhile, the AgNWs form a highly conductive network structure and effectively transfer electrons while maintaining a flexible structure that can withstand repeated bending strain. As a result, screen-printed MSCs using RuO_2-xH_2O@MXene-AgNWs nanocomposite inks exhibit a volumetric capacity of 864.2 F cm^{-3} at a scan rate of 1 mV s^{-1}, excellent cycling stability (90% retention after 10,000 cycles) and excellent flexibility[130] [Figure 5C].

Transfer printing

Transfer printing is a method of transferring the ink from one substrate to another. In direct transfer printing, the material is directly transferred from the original substrate to the target substrate, similar to the

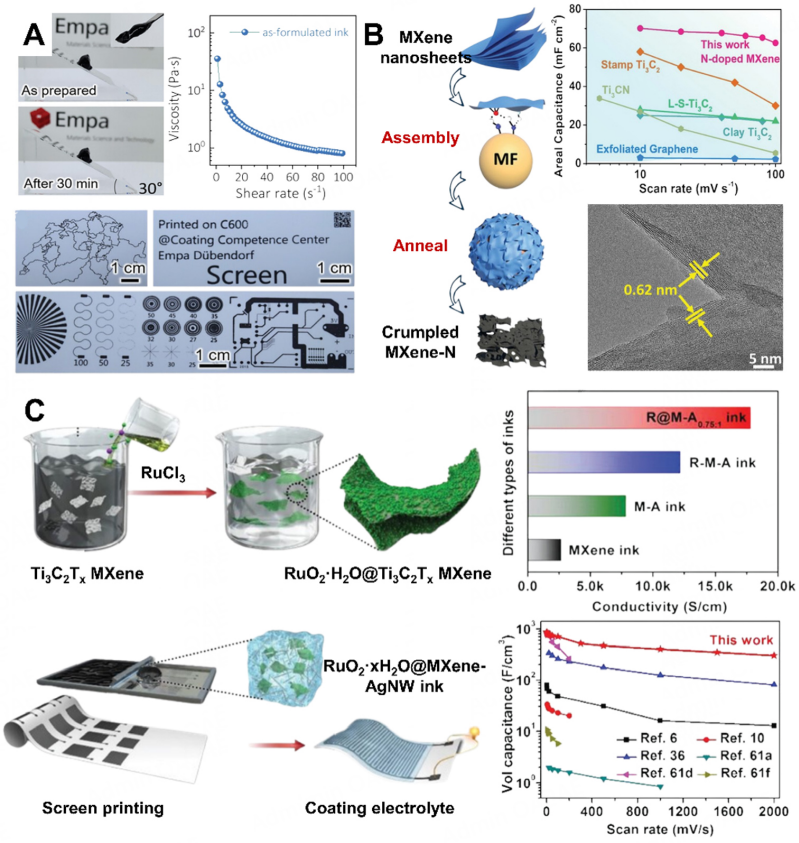

Figure 5. Screen printing of MXene inks. (A) The MXene sediment inks with shear thinning behavior for screen printed patterns. Reproduced with permission[128]. Copyright 2020, Wiley-VCH. (B) Schematic of synthesis of MXene-N and the HRTEM images of crumpled MXene-N nanosheets and comparison of the printed MSC areal capacitances under different scan rates from recently published studies. Reproduced with permission[105]. Copyright 2019, Wiley-VCH. (C) The synthesis of $RuO_2 \cdot xH_2O$@MXene nanocomposite. Reproduced with permission[130]. Copyright 2019, Wiley-VCH.

process of gravure printing. Therefore, this method does not require expensive/complex printing unit, and is suitable for many types of substrates. However, the ink printing process needs to be optimized to reduce the diffusion effect. In contrast, indirect transfer printing requires an intermediate transfer medium. This process involves four steps: first, the ink is deposited on the original substrate; second, an intermediate transfer medium, typically a flexible polymer, is chosen to transfer the ink from the original substrate; third, the intermediate transfer medium carrying the ink is transferred to the target substrate, and the ink is attached to the target substrate by certain methods; finally, the intermediate transfer medium and ink are stripped. Flexographic printing is the typical example of indirect transfer printing strategy. Indirect transfer printing typically results in a higher resolution than direct transfer printing. However, more complicated procedures suggest a higher cost for the indirect transfer printing.

The performance of transfer printing is influenced by a range of factors, including the characteristics of the substrate material and intermediate transfer medium, as well as environmental parameters such as temperature, atmosphere and pressure. By adjusting these parameters, it is possible to alter the binding forces between the ink and different substrates. To produce high-quality printed patterns, it is crucial that the bonding force between the ink and the intermediate transfer medium is stronger than the bonding force with the original substrate, but weaker than the bonding force with the target substrate[131]. MXene aqueous inks can be printed on a variety of substrates using stamps with various pattern designs[93]. Ultrathin MXene

micropatterns can be obtained by applying aqueous MXene ink to a polydimethylsiloxane (PDMS) stamp and then printed onto a coverslip, as shown in Figure 6A[132]. Zhang *et al.* have developed a method that uses aqueous inks ($Ti_3C_2T_x$ and Ti_3CNT_x) and transfer printing technology (with the help of a 3D-printed stamp) to fabricate flexible all-MXene MSCs[133]. $Ti_3C_2T_x$ MSCs with interdigitated fingers are produced by coating 3D-printed stamps with ink and then pressing them firmly onto flexible substrates, resulting in an areal capacitance of 61 mF cm^{-2} at 25 μA cm^{-2} and 50 mF cm^{-2} at 800 μA cm^{-2}. The stamping strategy is cost-effective and is capable of producing high-performance MXene-based MSCs on a large scale [Figure 6B].

3D printing

A 3D printing technology, also known as additive manufacturing technology, allows the creation of complex 3D objects without wasting materials by using designed structures. Fused deposition, photopolymerization, and direct ink writing (DIW) are typical 3D printing strategies. Currently, fused deposition modeling (FDM) is the most common 3D printing method. By repeatedly extruding functionalized ink from a nozzle, depositing it on a substrate, cooling and solidifying, 3D structures can be obtained. For production of miniature devices, the DIW process is an excellent method to transfer conductive inks to substrates, offering a low-cost and convenient solution for manufacturing electronic and energy storage devices[133]. This process can be categorized into two types: solid- and liquid-state writing. Solid-state writing involves the transfer of ink without solvent volatilization, whereas liquid writing uses the solvent volatilization to solidify the ink, which is dependent on the ink's wettability on the substrate. One of the primary advantages of the DIW process is that conductive inks can be directly deposited onto the substrate upon demand, thus no materials are wasted. The DIW technique is a simple and cost-effective printing method that allows the direct deposition of materials onto a variety of substrates. In addition, the emerging electrohydrodynamic printing technology, with its high resolution, wide range of materials and scalability, has shown great potential for development in the field of printed electronics.

Additive-free aqueous MXene inks with desirable viscoelastic properties were formulated for 3D printing of MSCs. Figure 7A illustrated the manufacturing process of aqueous MXene ink for 3D printing solid MSCs. The 3D structures were successfully fabricated by continuously extruding the additive-free aqueous MXene inks layer by layer [Figure 7B]. Well-defined shaped freestanding 3D structures were obtained after freeze-drying. The assembled solid-state symmetric MXene MSCs exhibited good capacitance, with an areal capacitance of the electrodes of 2.1 F cm^{-2} at an active material loading of about 8.5 mg cm^{-2}[134]. To enhance the electrochemical properties, the concentration of MXene inks can be increased by utilizing superabsorbent polymer (SAP) beads to realize the high concentration of $Ti_3C_2T_x$ inks (up to 290 mg/mL) [Figure 7C]. The highly conductive ink can be directly utilized for 3D printing of MSCs as both the current collector and active material for charge storage. Furthermore, the inks can be 3D-printed on a variety of substrates, including flexible polymers and paper. The printed MSCs exhibited excellent electrochemical properties, with an areal capacitance of up to 1,035 mF cm^{-2}[111].

Furthermore, by compositing MXene with other nanomaterials, composite inks can be formulated. For instance, Zhou *et al.* developed MXene/cellulose nanofibers (CNFs) composite inks and successfully printed various 3D structures at low MXene loadings[106]. CNFs were used as rheology modifiers to improve the rheological properties of MXene inks at low loading for more printability. Furthermore, the 3D-printed solid-state interdigitated symmetrical SCs were fabricated, exhibiting a high areal capacity (2.02 F cm^{-2} at 1 mA cm^{-2}), excellent rate capability (1.14 F cm^{-2} at 20 mA cm^{-2}), and good cycling stability of 85% over 5,000 cycles [Figure 7D].

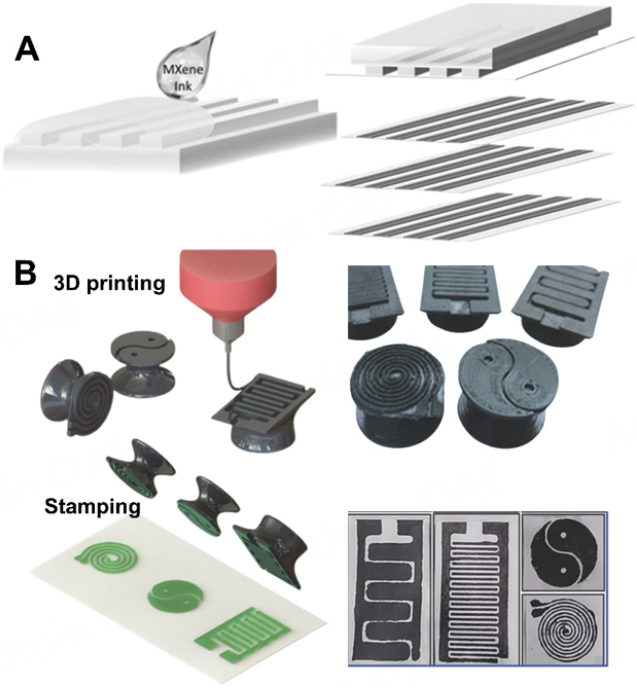

Figure 6. (A) Illustration of using microcontact printing (μCP) to print the ultrathin MXene micropatterns. Reproduced with permission[132]. Copyright 2016, Advanced Materials. (B) A 3D printing technology enables the creation of various stamp patterns and the use of stamps to fabricate MSCs by pressing them on the substrate. Reproduced with permission[51]. Copyright 2018, Wiley-VCH.

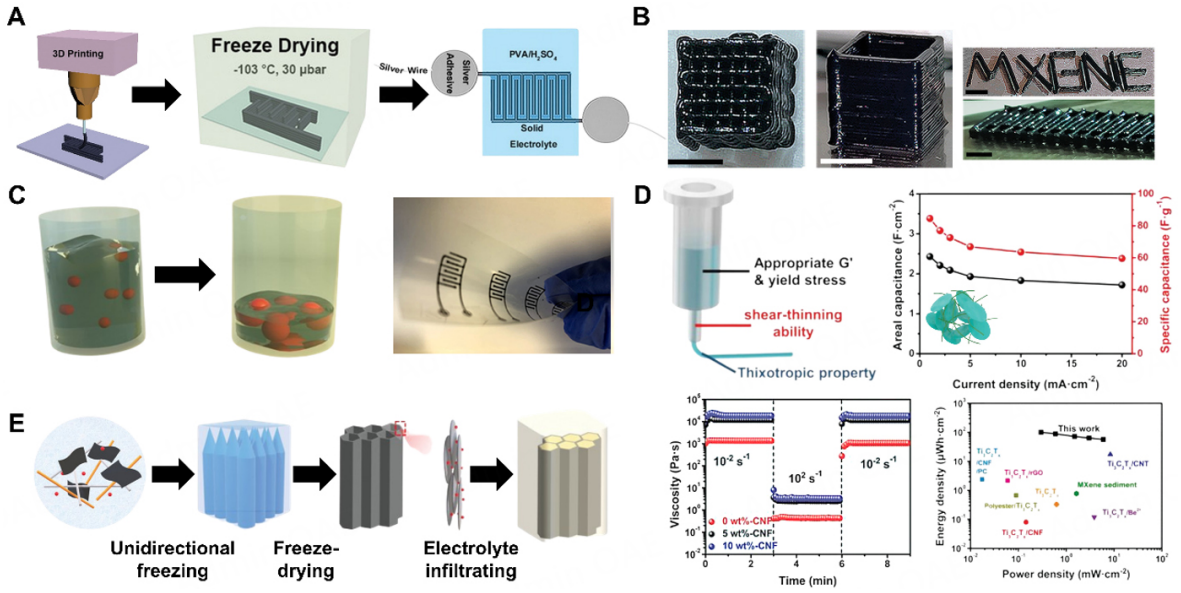

Figure 7. (A) Schematic of 3D-printed MSCs fabrication process. (B) Photographs of 3D-printed microlattice and rectangular hollow prism structures. Reproduced with permission[134]. Copyright 2019, John Wiley and Sons. (C) Schematic representation of the increase in MXene dispersion concentration due to the addition of SAP beads to absorb water. The printed MSC retains the complete pattern even after bending and twisting. Reproduced with permission[111]. Copyright 2019, American Chemical Society (D) Rheological properties of 3D printable gel inks and the electrochemical properties of the symmetric SC device. Reproduced with permission[106]. Copyright 2022, John Wiley and Sons. (E) The fabrication process of MSCs using 3D printing with unidirectional freezing. Reproduced with permission[135]. Copyright 2020, John Wiley and Sons.

A nanocomposite ink composed of MXene, manganese dioxide nanowires (MnONWs), AgNWs, and fullerene (C60) was reported for high-resolution 3D printing[135]. By mixing high capacitance MnONWs and highly conductive AgNWs, boosted charge transfer kinetics and improved electrochemical performance were achieved. In this composite ink, C60 acts as the lubricant, reducing friction between neighboring layers and allowing the MXene layer to stretch. The 3D-printed MSC ultimately experienced less than a 20% degradation in areal capacitance at up to 50% tensile strain and maintained approximately 75% of its initial capacitance after 1,000 stretch/release cycles [Figure 7E].

Coating methods

In addition to the printing methods discussed above, solution-based coating of MXene inks can also be employed to fabricate MXene conductive patterns. Unlike printing techniques, coating methods require less stringent ink rheological properties and equipment. Conventional coating methods include spray coating, blade coating, spin coating, slot die coating, *etc.*[33,136-138].

Spray coating works based on the ejection of MXene ink using pressurized carrier gas from a spray gun through a nozzle, resulting in an aerosol that rapidly dried upon depositing on the substrate, forming large-area conductive films. Factors such as solvent type, velocity, distance between the substrate and the nozzle and temperature all affect the uniformity of the obtained film. Xie *et al.* developed high-voltage asymmetric, on-chip MXene MSCs using $Ti_3C_2T_x$ as the negative electrode and activated carbon as the positive electrode with a simple cutting-spraying method[139]. Results showed that the prepared MSCs can operate at a wide voltage window of 1.6 V and deliver 3.5 mWh cm^{-3} (with a power density of 100 mW cm^{-3}), which is superior to reported on-chip energy storage devices. Besides, the MSCs exhibit good capacitance retention of ~91.4% after 10,000 cycles [Figure 8A].

Blade coating is a versatile and scalable method that has been extensively studied due to its simplicity. In this method, the ink is deposited onto the substrate in front of the blade and then moved across the substrate to form uniform, large-area thin films. The thickness of the film obtained by blade coating varies based on the speed of the blade, the distance between the blade and substrate, the substrate wettability, and the viscosity of the ink[140]. Using the blade coating technique, $Ti_3C_2T_x$ films have been reported as transparent conductive electrodes (TCEs) with excellent optoelectronic properties (19,325 S cm^{-1}). Based on $Ti_3C_2T_x$ TCEs, the electrochemical properties of MSCs were investigated, with a maximum energy density of 0.004 μWh cm^{-2} (at a power density of 0.23 μW cm^{-2}) and maintaining 90% of their initial capacity after 10,000 cycles[141] [Figure 8B].

Similar to blade coating, slot-die coating is a very versatile coating technique in which a solution is delivered to the substrate and deposits to form films through a narrow slot with thicknesses ranging from a few nanometres to a few micrometers. The advantages of the technique lie mainly in the fact that the films can be produced on a large scale and are suitable for different solvent types and viscosities. By carefully regulating the speed of coating and the height of the gaps, it is possible to form highly aligned, compact films with a high degree of homogeneity. For instance, Guo *et al.* optimized the rheological properties of MXene aqueous inks to produce large-area, low-roughness films at RT, and then used direct laser scribing to fabricate MSCs[142]. It is noted that the rate performance of the thick film is poor due to its highly compact and aligned flake, which impedes the ion transport kinetics [Figure 8C]. On the other hand, vacuum-assisted filtration is the easiest way to produce MXene freestanding films with a desired thickness. For instance, MXene MSCs can also be fabricated by mask-assisted vacuum filtration. However, the limited filtration speed and filter size, as well as the subsequent transfer process, renders this approach difficult to scale up[143] [Figure 8D].

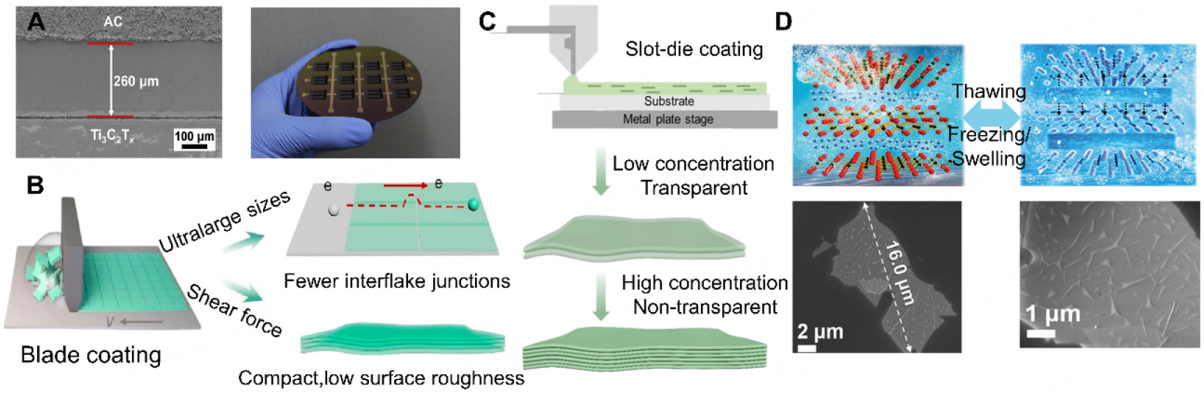

Figure 8. Coating methods. (A) SEM image of interdigital gap for on-chip MSCs manufactured by cutting-spraying method and digital photograph of integrating MXene-based on-chip MSCs. Reproduced with permission[139]. Copyright 2020, Elsevier. (B) By blade coating with large flake of MXene aqueous ink, a high conductivity film can be produced. Reproduced with permission[141]. Copyright 2023, American Chemical Society. (C)Slot die coating of transparent and non-transparent films on different substrates. Reproduced with permission[142]. Copyright 2023, John Wiley and Sons. (D) The preparation of the delaminated-Ti_3C_2 via the freeze-and-thaw (FAT) method and SEM images of delaminated-Ti_3C_2 with obvious wrinkles on the surface. Reproduced with permission[143]. Copyright 2020, Wiley-VCH.

PRINTED ENERGY STORAGE DEVICES BEYOND MSCS

The unique structure and high conductivity of MXene allow it to be employed as a conductive host for anodes in rechargeable batteries[144]. Lithium metal is considered as an ideal anode for rechargeable lithium-based batteries due to its low redox potential (-3.04 V *vs.* the standard hydrogen electrode) and high theoretical capacity (3,860 mAh g^{-1})[145]. Nevertheless, the low Coulombic efficiency, the irregular solid electrolyte interphase (SEI) deposition and uncontrollable growth of lithium dendrites in lithium-metal batteries pose great safety risks[146]. The safety of lithium-based batteries is determined by whether the lithium dendrites formation is under control. Indeed, these dendrites are formed due to the uncontrolled electrochemical deposition of lithium ions on the negative side of the lithium metal, and their sharp tips can not only pierce the battery diaphragm, but also short circuits the positive and negative battery electrodes, causing explosion and combustion. Therefore, finding ways to prevent the formation of dendrites and improve the safety of lithium-ion batteries (LIBs) is crucial for their successful development and widespread application.

By constructing 3D MXene scaffolds, the volume expansion can be suppressed and homogeneous local current distribution in MXene-Li composite is facilitated, which is of critical significance in prolonging the lithium-metal batteries life and improving the safety.

For instance, Shen *et al.* used 3D-printed MXene arrays with wide gaps to prepare lithium anodes [Figure 9A][147]. These arrays effectively facilitated lithium nucleation, guided parallel lithium growth along the filaments, ensured uniform Li^+ flux and electric field, and prevented dendrites growth during repeated plating/stripping. Even after 1,200 h of cycling, the MXene arrays still showed no significant lithium dendrites, demonstrating their potential for application in 3D-printed lithium-based batteries. Similarly, vertically aligned $Ti_3C_2T_x$ electrodes have also been reported[148]. Compared with the closely stacked horizontal structure of $Ti_3C_2T_x$ nanosheets, the vertically aligned MXene allows for fast passage of Li^+ through the channels, uniform deposition after electrochemical reduction, and enrichment of the active surface area for Li deposition, thus facilitating dendrite-free growth and enhancing rate performance [Figure 9B]. The vertically aligned $Ti_3C_2T_x$ electrode achieved a high coulombic efficiency (98.8%) for more than 450 cycles at a fixed surface capacity of 1.0 mAh cm^{-2} and a current density of 1.0 mA cm^{-2}. Notably,

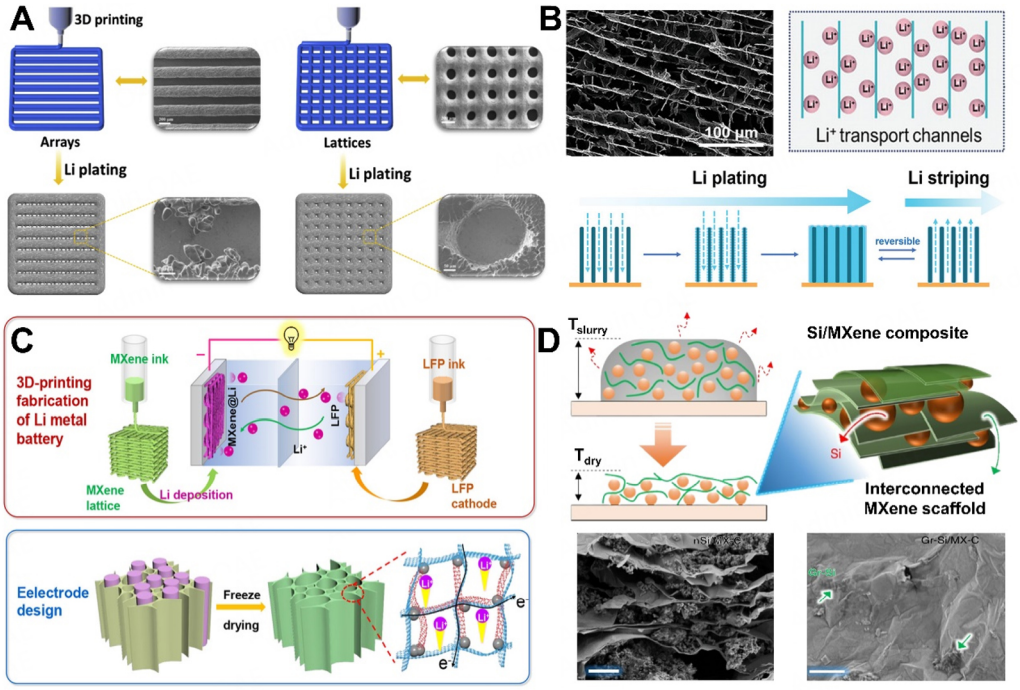

Figure 9. (A) Schematic of 3D-printed MXene arrays and lattices. Reproduced with permission[147]. Copyright 2020, Elsevier. (B) Schematic and coulombic efficiency plots of the lithium plating/stripping behavior of vertical MXene electrodes at 1.0 mA cm^{-2} and SEM image of v-$Ti_3C_2T_x$ electrodes. Reproduced with permission[148]. Copyright 2022, Wiley-VCH. (C) Diagram of 3D-printed LMB. Working principle of printing MXene scaffold and super-thick LFP lattice for LMB (top), freeze-drying prepare of porous MXene lattices (bottom). Reproduced with permission[149]. Copyright 2023, Elsevier. (D) Preparation process and rheological properties of Si/MXene inks and SEM images of nSi/MX-C electrode and Gr-Si/MX-C electrode. Reproduced with permission[152]. Copyright 2019, Springer Nature.

when paired with a $LiFePO_4$ (LFP) cathode, the vertically aligned $Ti_3C_2T_x$ electrode exhibited better performance than the horizontally aligned electrode, achieving a stable cycling performance of 300 cycles at 0.5 C with a capacity retention rate of 85.4%.

To enhance the performance of lithium-based batteries, a multi-dimensional LFP was developed as an ultra-thick cathode by 3D printing[149]. The cathode was assembled with a dendrite-free MXene@Li anode, achieving unprecedented areal capacity (25.3 mAh cm^{-2}) and energy density (81.6 mWh cm^{-2}) at an ultra-high mass loading of 171 mg cm^{-2}, exceeding all reported 3D-printed batteries [Figure 9C].

In addition to lithium anodes, silicon-based anodes have received a lot of attention due to their superior theoretical capacity and abundant reserves, but the volumetric expansion caused by the lithiation process can crack the surface of the material and reduce the capacity[150,151]. Viscous $Ti_3C_2T_x$ (MX-C) inks have been reported as conductive binders for the manufacture of Si/MXene anodes with high mass loading and hence high areal capacitance[152]. The MXene nanosheets in the prepared MX-C inks formed a continuous conductive network that enwrapped the Si nanoparticles, resulting in electrodes with excellent mechanical properties and the ability to produce thick electrodes [Figure 9D]. Compared to conventional additives, the thickness of the MX-C ink could reach ~350 μm before cracking occurs, while the critical cracking thickness (CCT) of conventional additives was less than 100 μm. This is due to the much higher apparent viscosity of MX-C than that of conventional two-component additives such as polyacrylic acid/carbon black (PAA/CB)-water system. Besides, the electrochemical properties of the composite electrodes were investigated. The results indicated that nanoscale Si (nSi)/MX-C exhibited good stability after 280 cycles of charging and

discharging. The electrode could adapt well to changes in volume and maintain a good electron transport network, thereby addressing the stability problem of conventional polymeric binders.

The challenges of lithium-sulfur batteries include the insulating nature of sulfur and the shuttling effect of the soluble polysulfides[153]. To address these challenges, Tang *et al.* reported a viscous aqueous ink with nanoscale S uniformly decorated on titanium carbide MXene nanosheets (S@$Ti_3C_2T_x$)[154]. The conductive $Ti_3C_2T_x$ effectively chemisorbed soluble lithium polysulfide, forming a thick sulfate layer that significantly suppresses the polysulfide shuttling during cycling and improves sulfur utilization. Eventually, S@$Ti_3C_2T_x$ exhibited high capacity at all C-rates, excellent rate handling, and ultra-low capacity decay rate [Figure 10A]. Similarly, the preparation of nitrogen-doped porous Ti_3C_2 MXene (N-p $Ti_3C_2T_x$) frameworks that regulate both S cathodes and Li anodes using 3D printing techniques has also been reported[155]. This framework possesses a hierarchical porous structure, high electrical conductivity, and structural robustness, endowing it with the lithiophilic-sulfiphilic property and the ability to provide fast charge transport while inhibiting polysulfide shuttle and dendrite growth. As a result, the printed Li-S full cells (3DP N-p $Ti_3C_2T_x$/S||3DP N-p $Ti_3C_2T_x$ @Li) can operate continuously for 60 cycles at 12.02 mg cm^{-2} with a cycling capacity of 8.47 mAh cm^{-2} [Figure 10B]. Table 3 summarized the reviewed printed/coated Mxene-based batteries.

Alternatively, MXene inks can be coated for conductive substrates. For instance, the researchers developed a new gelation-assisted method for the formulation of versatile MXene gel ink, which exhibited improved rheological properties. In addition, the MXene anode prepared by blade coating showed[158] uniform zinc deposition and high plating/stripping reversibility with coulombic efficiency values of up to 99.7% at a high rate of 20 mA cm^{-2}. The assembled aqueous zinc ion batteries exhibited a high capacitance retention of 90% after 100 cycles at a rate of 2 A g^{-1}.

Besides, separator modification is an effective strategy for dendrite-free zinc anodes. For instance, an MXene-decorated separator by spray-printing MXene inks on one side of a commercial glass fiber (GF) has been reported[162]. The abundant surface polar groups, good electrolyte wettability, and high ionic conductivity of the MXene-GF separator facilitate uniform local current distribution and promote zinc nucleation kinetics. The full cell of the aqueous zinc ion battery assembled with Janus MXene-GF separator maintained 77.9% capacity after 1,000 cycles at 5.0 A g^{-1}. In addition, there is an urgent need to develop micro-batteries with high power and energy density. Micro-batteries based on MXene ink printing have been reported to exhibit excellent electrochemical properties. For example, VS_2/MXene cathodes have been successfully designed for aqueous micro zinc ion batteries, exhibiting high capacitance and excellent cycle life.

SUMMARY AND PERSPECTIVES

In summary, MXenes have been intensively investigated in the printed energy storage field owing to their excellent electrochemical charge storage performances, mechanical/electrical properties, and, in particular, the excellent solution processability of MXene inks. So far, a variety of methods have been investigated to fabricate MXene MSCs by employing the charge storage or electrical properties, respectively. However, the development of large-scale, reproducible and cost-effective printing/coating processes for MXene inks remains a major challenge for the commercial production of high-performance EESDs. Most critically, scaling up the production of MXene inks and improving their stability to meet industrial demand are major challenges for commercial applications. To meet industrial requirements, novel methods, such as supercritical carbon dioxide-assisted etching or gaseous assembly of MXene flakes, should be further developed with kg yields. In addition, improving the oxidative stability of inks should also be the priority when considering the scale-up of the application of MXene inks toward printed energy storage devices and beyond.

Table 3. The performance of printed/coated MXene-based batteries for EESDs

Refs.	Printing/coating methods	Type	Electrodes	Electrolyte	Performance
[156]	Inkjet printing	Li-ion batteries	Lithium//V_2O_5/$Ti_3C_2T_x$	$LiPF_6$	112 mAh g^{-1}, 680 cycles (91.8%)
[147]	3D printing	Li-ion batteries	$Ti_3C_2T_x$ arrays-Li//LFP	$LiPF_6$	149.4 mAh g^{-1}, 300 cycles (99.4%)
[157]	Blade coating	Li-ion batteries	LTO/$Ti_3C_2T_x$//NMC/$Ti_3C_2T_x$	$LiPF_6$	154 mAh g^{-1}, 200 cycles (101.4%)
[152]	Slurry casting	Li-ion batteries	Si/$Ti_3C_2T_x$//Lithium	$LiPF_6$	23.3 mAh cm^{-2}
[155]	3D printing	Li-S batteries	N-p$Ti_3C_2T_x$@Li//N-p$Ti_3C_2T_x$ /S	LiTFSI/$LiNO_3$	8.47 mAh cm^{-2}, 250 cycles (decay of 0.06% per cycle)
[154]	Vacuum filtration	Li-S batteries	Lithium//S@$Ti_3C_2T_x$	LiTFSI/$LiNO_3$	1,350 mAh g^{-1}, 175 cycles (decay of 0.035% per cycle)
[148]	Blade coating	Lithium metal batteries	Li@v-$Ti_3C_2T_x$//LFP	LiTFSI/$LiNO_3$	135 mAh g^{-1}, 300 cycles (85.4%)
[158]	Blade coating	Zinc ion batteries	Zn-$Ti_3C_2T_x$//NVO	$ZnSO_4$/Na_2SO_4	4 mAh cm^{-2}, 100 cycles (90%)
[159]	Patterning	Zn metal batteries	$Ti_3C_2T_x$@Zn//MnO_2	$ZnSO_4$/$MnSO_4$	281.9 mA h g^{-1}, 200 cycles (79.7%)
[160]	3D printing	Na metal batteries	Na@V_2CT_x/rGO-CNT//NVP@C-rGO	$NaPF_6$ in diglyme	400 cycles (86.27%)
[161]	3D printing	Sodium metal batteries	Na@$Ti_3C_2T_x$ /rGO//NVP@C-rGO	$NaPF_6$ in diglyme	500 cycles (85.3%)

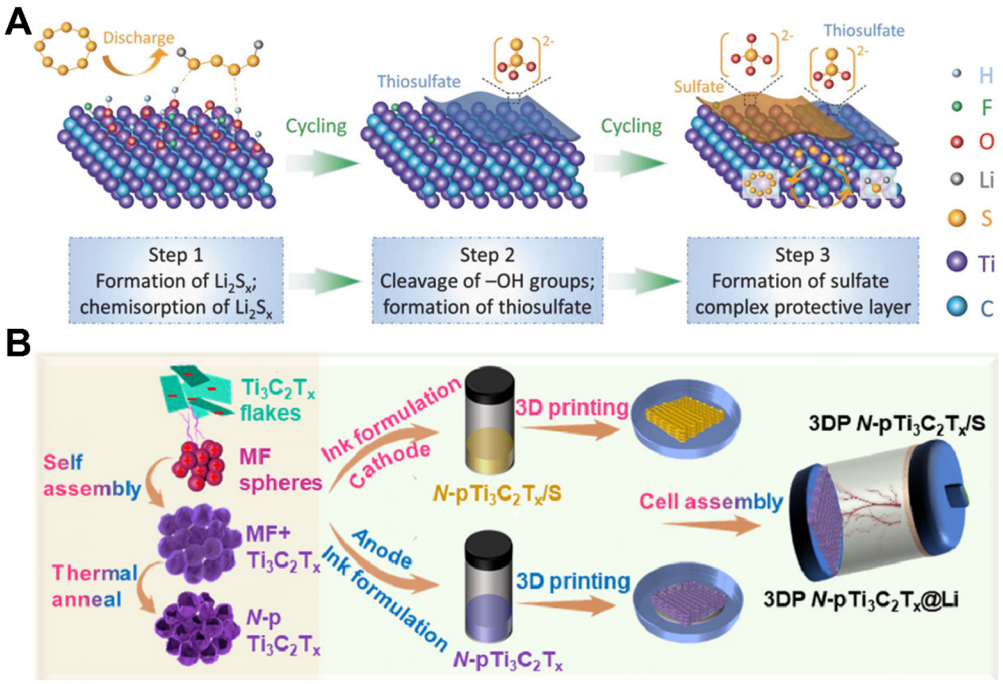

Figure 10. (A) Schematic demonstration of $Ti_3C_2T_x$ entrapping the polysulfides by forming a sulfate complex protective barrier. (B) The preparation process of LSB dual electrodes by 3D printing framework with N-p $Ti_3C_2T_x$. Reproduced with permission[154]. Copyright 2018, John Wiley and Sons. Reproduced with permission[155]. Copyright 2021, Elsevier.

It should be highlighted that synthesizing MXene with controllable and uniform surface terminations is of significance but quite challenging. Currently, researchers have found that the surface terminations affect the lithium-ion flux and diffusion kinetics, resulting in the controllable deposition of SEI layers and suppressing the lithium dendrites formation if proper MXene surface terminations are achieved. Moreover, these surface terminations have important implications for the rheological properties, film formation, and device performance of MXene inks. The precise tuning of MXene surface chemistries should also benefit the film adhesion.

Finally, the EESD integration based on MXene with other sensors or energy conversion allows the development of more functions, opening vast opportunities of MXenes. For example, by integrating self-powered device nanogenerators with MXene EESDs, continuous energy supply can be achieved from the wind to meet the electricity demand in specific areas. Integration with sensors is also a promising direction. The integrated device does not require an external power source for charging, improving its flexibility. We are quite optimistic that through continuous investigation of MXenes, more killer applications can be unleashed very soon.

DECLARATIONS

Authors' contributions

Selecting the topic of review, funding acquisition and supervision: Zhang, C.
Investigation and analysis: He, Q.; Chen, H.; Chen, Y.; Zeng, C.
Writing and editing the review: Li, Z.; Xu, T.
Revising the review: Deng, S.

Availability of data and materials

Not applicable.

Financial support and sponsorship

Zhang, C. thanks the generous support from the Fundamental Research Funds for the Central Universities (1082204112A26), the National Natural Science Foundation of China (22209118), and the Open Research Fund of the State Key Laboratory of Mesoscience and Engineering (MESO-23-D06).

Conflicts of interest

All authors declared that there are no conflicts of interest.

Ethical approval and consent to participate

Not applicable.

Consent for publication

Not applicable.

Copyright

© The Author(s) 2025.

REFERENCES

1. Larcher, D.; Tarascon, J. M. Towards greener and more sustainable batteries for electrical energy storage. *Nat. Chem.* **2015**, *7*, 19-29. DOI PubMed
2. Huang, J.; Xie, Y.; You, Y.; et al. Rational design of electrode materials for advanced supercapacitors: from lab research to commercialization. *Adv. Funct. Mater.* **2023**, *33*, 2213095. DOI

3. Zhang, Y.; Mei, H. X.; Cao, Y.; et al. Recent advances and challenges of electrode materials for flexible supercapacitors. *Coord. Chem. Rev.* **2021**, *438*, 213910. DOI
4. Keum, K.; Kim, J. W.; Hong, S. Y.; Son, J. G.; Lee, S. S.; Ha, J. S. Flexible/stretchable supercapacitors with novel functionality for wearable electronics. *Adv. Mater.* **2020**, *32*, e2002180. DOI PubMed
5. Pomerantseva, E.; Bonaccorso, F.; Feng, X.; Cui, Y.; Gogotsi, Y. Energy storage: the future enabled by nanomaterials. *Science* **2019**, *366*, eaan8285. DOI PubMed
6. Zhang, Y. Z.; Wang, Y.; Cheng, T.; et al. Printed supercapacitors: materials, printing and applications. *Chem. Soc. Rev.* **2019**, *48*, 3229-64. DOI
7. Lethien, C.; Le, B. J.; Brousse, T. Challenges and prospects of 3D micro-supercapacitors for powering the internet of things. *Energy. Environ. Sci.* **2019**, *12*, 96-115. DOI
8. Tian, Y.; An, Y.; Feng, J.; Qian, Y. MXenes and their derivatives for advanced aqueous rechargeable batteries. *Mater. Today.* **2022**, *52*, 225-49. DOI
9. Dunn, B.; Kamath, H.; Tarascon, J. M. Electrical energy storage for the grid: a battery of choices. *Science* **2011**, *334*, 928-35. DOI PubMed
10. Salanne, M.; Rotenberg, B.; Naoi, K.; et al. Efficient storage mechanisms for building better supercapacitors. *Nat. Energy.* **2016**, *1*, 16070. DOI
11. Chen, G. Z. Supercapacitor and supercapattery as emerging electrochemical energy stores. *Int. Mater. Rev.* **2017**, *62*, 173-202. DOI
12. Sheberla, D.; Bachman, J. C.; Elias, J. S.; Sun, C. J.; Shao-Horn, Y.; Dincă, M. Conductive MOF electrodes for stable supercapacitors with high areal capacitance. *Nat. Mater.* **2017**, *16*, 220-4. DOI PubMed
13. Zheng, S.; Huang, H.; Dong, Y.; et al. Ionogel-based sodium ion micro-batteries with a 3D Na-ion diffusion mechanism enable ultrahigh rate capability. *Energy. Environ. Sci.* **2020**, *13*, 821-9. DOI
14. Simon, P.; Gogotsi, Y. Perspectives for electrochemical capacitors and related devices. *Nat. Mater.* **2020**, *19*, 1151-63. DOI PubMed
15. Tan, C.; Cao, X.; Wu, X. J.; et al. Recent advances in ultrathin two-dimensional nanomaterials. *Chem. Rev.* **2017**, *117*, 6225-331. DOI
16. Zeraati A, Mirkhani SA, Sun P, Naguib M, Braun PV, Sundararaj U. Improved synthesis of $Ti_3C_2T_x$ MXenes resulting in exceptional electrical conductivity, high synthesis yield, and enhanced capacitance. *Nanoscale* **2021**, *13*, 3572-80. DOI PubMed
17. Lipatov, A.; Lu, H.; Alhabeb, M.; et al. Elastic properties of 2D $Ti_3C_2T_x$ MXene monolayers and bilayers. *Sci. Adv.* **2018**, *4*, eaat0491. DOI
18. Maleski, K.; Shuck, C. E.; Fafarman, A. T.; Gogotsi, Y. The broad chromatic range of two-dimensional transition metal carbides. *Adv. Opt. Mater.* **2021**, *9*, 2001563. DOI
19. Manzeli, S.; Ovchinnikov, D.; Pasquier, D.; Yazyev, O. V.; Kis, A. 2D transition metal dichalcogenides. *Nat. Rev. Mater.* **2017**, *2*, 17033. DOI
20. Munkhbat, B.; Yankovich, A. B.; Baranov, D. G.; Verre, R.; Olsson, E.; Shegai, T. O. Transition metal dichalcogenide metamaterials with atomic precision. *Nat. Commun.* **2020**, *11*, 4604. DOI PubMed PMC
21. Zhao, J.; Liu, H.; Yu, Z.; et al. Rise of silicene: a competitive 2D material. *Prog. Mater. Sci.* **2016**, *83*, 24-151. DOI
22. Molle, A.; Grazianetti, C.; Tao, L.; Taneja, D.; Alam, M. H.; Akinwande, D. Silicene, silicene derivatives, and their device applications. *Chem. Soc. Rev.* **2018**, *47*, 6370-87. DOI
23. Lv, L.; Yang, Z.; Chen, K.; Wang, C.; Xiong, Y. 2D layered double hydroxides for oxygen evolution reaction: from fundamental design to application. *Adv. Energy. Mater.* **2019**, *9*, 1803358. DOI
24. Hu, T.; Gu, Z.; Williams, G. R.; et al. Layered double hydroxide-based nanomaterials for biomedical applications. *Chem. Soc. Rev.* **2022**, *51*, 6126-76. DOI
25. Lin, Z.; Wang, C.; Chai, Y. Emerging group-VI elemental 2D materials: preparations, properties, and device applications. *Small* **2020**, *16*, e2003319. DOI
26. Qiu, M.; Ren, W. X.; Jeong, T.; et al. Omnipotent phosphorene: a next-generation, two-dimensional nanoplatform for multidisciplinary biomedical applications. *Chem. Soc. Rev.* **2018**, *47*, 5588-601. DOI
27. Lin, Z.; Li, X.; Zhang, H.; et al. Research progress of MXenes and layered double hydroxides for supercapacitors. *Inorg. Chem. Front.* **2023**, *10*, 4358-92. DOI
28. Lamiel, C.; Hussain, I.; Warner, J. H.; Zhang, K. Beyond Ti-based MXenes: a review of emerging non-Ti based metal-MXene structure, properties, and applications. *Mater. Today.* **2023**, *63*, 313-38. DOI
29. Gogotsi, Y.; Anasori, B. The rise of MXenes. *ACS. Nano.* **2019**, *13*, 8491-4. DOI PubMed
30. Naguib, M.; Kurtoglu, M.; Presser, V.; et al. Two-dimensional nanocrystals produced by exfoliation of Ti_3AlC_2. *Adv. Mater.* **2011**, *23*, 4248-53. DOI
31. Anasori, B.; Lukatskaya, M. R.; Gogotsi, Y. 2D metal carbides and nitrides (MXenes) for energy storage. *Nat. Rev. Mater.* **2017**, *2*, 1-17. DOI
32. Sinha, A.; Dhanjai; Zhao, H.; et al. MXene: an emerging material for sensing and biosensing. *TrAC. Trends. Anal. Chem.* **2018**, *105*, 424-35. DOI
33. Hantanasirisakul, K.; Zhao, M. Q.; Urbankowski, P.; et al. Fabrication of $Ti_3C_2T_x$ MXene transparent thin films with tunable optoelectronic properties. *Adv. Elect. Mater.* **2016**, *2*, 1600050. DOI
34. Hantanasirisakul, K.; Gogotsi, Y. Electronic and optical properties of 2D transition metal carbides and nitrides (MXenes). *Adv.*

Mater. **2018**, *30*, e1804779. DOI PubMed

35. Huang, H.; Jiang, R.; Feng, Y.; et al. Recent development and prospects of surface modification and biomedical applications of MXenes. *Nanoscale* **2020**, *12*, 1325-38. DOI PubMed
36. Gao, G.; O'mullane, A. P.; Du, A. 2D MXenes: a new family of promising catalysts for the hydrogen evolution reaction. *ACS. Catal.* **2017**, *7*, 494-500. DOI
37. Yang, R.; Fan, Y.; Mei, L.; et al. Synthesis of atomically thin sheets by the intercalation-based exfoliation of layered materials. *Nat. Synth.* **2023**, *2*, 101-18. DOI
38. Li, J.; Ye, F.; Vaziri, S.; Muhammed, M.; Lemme, M. C.; Östling, M. Efficient inkjet printing of graphene. *Adv. Mater.* **2013**, *25*, 3985-92. DOI
39. Li, J.; Sollami, D. S.; Zhang, P.; et al. Scalable fabrication and integration of graphene microsupercapacitors through full inkjet printing. *ACS. Nano.* **2017**, *11*, 8249-56. DOI
40. Jun, H. Y.; Ryu, S. O.; Kim, S. H.; et al. Inkjet printing of few-layer enriched black phosphorus nanosheets for electronic devices. *Adv. Elect. Mater.* **2021**, *7*, 2100577. DOI
41. Li, L.; Meng, J.; Bao, X.; et al. Direct-ink-write 3D printing of programmable micro-supercapacitors from MXene-regulating conducting polymer inks. *Adv. Energy. Mater.* **2023**, *13*, 2203683. DOI
42. Shao, Y.; Wei, L.; Wu, X.; et al. Room-temperature high-precision printing of flexible wireless electronics based on MXene inks. *Nat. Commun.* **2022**, *13*, 3223. DOI PubMed PMC
43. Zhu, Q.; Li, J.; Simon, P.; Xu, B. Two-dimensional MXenes for electrochemical capacitor applications: progress, challenges and perspectives. *Energy. Stor. Mater.* **2021**, *35*, 630-60. DOI
44. Azadmanjiri, J.; Reddy, T. N.; Khezri, B.; et al. Prospective advances in MXene inks: screen printable sediments for flexible micro-supercapacitor applications. *J. Mater. Chem. A.* **2022**, *10*, 4533-57. DOI
45. Vural, M.; Pena-Francesch, A.; Bars-Pomes, J.; et al. Inkjet printing of self-assembled 2D titanium carbide and protein electrodes for stimuli-responsive electromagnetic shielding. *Adv. Funct. Mater.* **2018**, *28*, 1801972. DOI
46. Jiang, X.; Li, W.; Hai, T.; et al. Inkjet-printed MXene micro-scale devices for integrated broadband ultrafast photonics. *NPJ. 2D. Mater. Appl.* **2019**, *3*, 34. DOI
47. Yu, Z.; Deng, C.; Sun, J.; et al. Cellulosic nonwovens incorporated with fully utilized MXene precursor as smart pressure sensor and multi-protection materials. *Adv. Funct. Mater.* **2024**, 2402707. DOI
48. Wu, H.; Xie, Y.; Ma, Y.; et al. Aqueous MXene/xanthan gum hybrid inks for screen-printing electromagnetic shielding, joule heater, and piezoresistive sensor. *Small* **2022**, *18*, e2107087. DOI
49. Pan, S.; Yin, J.; Yu, L.; et al. 2D MXene-integrated 3D-printing scaffolds for augmented osteosarcoma phototherapy and accelerated tissue reconstruction. *Adv. Sci.* **2020**, *7*, 1901511. DOI PubMed PMC
50. Cao, W. T.; Ma, C.; Mao, D. S.; Zhang, J.; Ma, M. G.; Chen, F. MXene-reinforced cellulose nanofibril inks for 3D-printed smart fibres and textiles. *Adv. Funct. Mater.* **2019**, *29*, 1905898. DOI
51. Zhang, C.; Kremer, M. P.; Seral-Ascaso, A.; et al. Stamping of flexible, coplanar micro-supercapacitors using MXene inks. *Adv. Funct. Mater.* **2018**, *28*, 1705506. DOI
52. Zhang, C. J.; McKeon, L.; Kremer, M. P.; et al. Additive-free MXene inks and direct printing of micro-supercapacitors. *Nat. Commun.* **2019**, *10*, 1795. DOI PubMed PMC
53. Zhang, Y. Z.; Wang, Y.; Jiang, Q.; El-Demellawi, J. K.; Kim, H.; Alshareef, H. N. MXene printing and patterned coating for device applications. *Adv. Mater.* **2020**, *32*, e1908486. DOI
54. Akuzum, B.; Maleski, K.; Anasori, B.; et al. Rheological characteristics of 2D titanium carbide (MXene) dispersions: a guide for processing MXenes. *ACS. Nano.* **2018**, *12*, 2685-94. DOI
55. Xu, S.; Dall'Agnese, Y.; Wei, G.; Zhang, C.; Gogotsi, Y.; Han, W. Screen-printable microscale hybrid device based on MXene and layered double hydroxide electrodes for powering force sensors. *Nano. Energy.* **2018**, *50*, 479-88. DOI
56. Zheng, S.; Ma, J.; Fang, K.; et al. High-voltage potassium ion micro-supercapacitors with extraordinary volumetric energy density for wearable pressure sensor system. *Adv. Energy. Mater.* **2021**, *11*, 2003835. DOI
57. Zheng, S.; Wang, H.; Das, P.; et al. Multitasking MXene inks enable high-performance printable microelectrochemical energy storage devices for all-flexible self-powered integrated systems. *Adv. Mater.* **2021**, *33*, e2005449. DOI
58. Zhang, Y.; Wang, L.; Zhao, L.; et al. Flexible self-powered integrated sensing system with 3D periodic ordered black phosphorus@MXene thin-films. *Adv. Mater.* **2021**, *33*, e2007890. DOI
59. Levitt, A.; Hegh, D.; Phillips, P.; et al. 3D knitted energy storage textiles using MXene-coated yarns. *Mater. Today.* **2020**, *34*, 17-29. DOI
60. Jiang, Q.; Kurra, N.; Maleski, K.; et al. On-chip MXene microsupercapacitors for AC-line filtering applications. *Adv. Energy. Mater.* **2019**, *9*, 1901061. DOI
61. Hong, S. Y.; Sun, Y.; Lee, J.; et al. 3D printing of free-standing $Ti_3C_2T_x$/PEO architecture for electromagnetic interference shielding. *Polymer* **2021**, *236*, 124312. DOI
62. Geng, D.; Zhao, X.; Chen, Z.; et al. Direct synthesis of large-area 2D Mo_2C on in situ grown graphene. *Adv. Mater.* **2017**, *29*, 1700072. DOI
63. Geng, D.; Zhao, X.; Li, L.; et al. Controlled growth of ultrathin Mo_2C superconducting crystals on liquid Cu surface. *2D. Mater.* **2017**, *4*, 011012. DOI

64. Wang, D.; Zhou, C.; Filatov, A. S.; et al. Direct synthesis and chemical vapor deposition of 2D carbide and nitride MXenes. *Science* **2023**, *379*, 1242-7. DOI
65. Xiang, M.; Shen, Z.; Zheng, J.; et al. Gas-phase synthesis of Ti_2CCl_2 enables an efficient catalyst for lithium-sulfur batteries. *Innovation* **2024**, *5*, 100540. DOI PubMed PMC
66. Alhabeb, M.; Maleski, K.; Mathis, T. S.; et al. Selective etching of silicon from Ti_3SiC_2 (MAX) To obtain 2D titanium carbide (MXene). *Angewe. Chem. Intl. Ed.* **2018**, *130*, 5542-6. DOI
67. Wang, L.; Zhang, H.; Wang, B.; et al. Synthesis and electrochemical performance of $Ti_3C_2T_x$ with hydrothermal process. *Electron. Mater. Lett.* **2016**, *12*, 702-10. DOI
68. Li, T.; Yan, X.; Huang, L.; et al. Fluorine-free $Ti_3C_2T_x$ (T = O, OH) nanosheets (~50-100 nm) for nitrogen fixation under ambient conditions. *J. Mater. Chem. A.* **2019**, *7*, 14462-5. DOI
69. Li, Y.; Shao, H.; Lin, Z.; et al. A general Lewis acidic etching route for preparing MXenes with enhanced electrochemical performance in non-aqueous electrolyte. *Nat. Mater.* **2020**, *19*, 894-9. DOI
70. Pang, S. Y.; Wong, Y. T.; Yuan, S.; et al. Universal strategy for HF-free facile and rapid synthesis of two-dimensional MXenes as multifunctional energy materials. *J. Am. Chem. Soc.* **2019**, *141*, 9610-6. DOI
71. Lim, K. R. G.; Shekhirev, M.; Wyatt, B. C.; Anasori, B.; Gogotsi, Y.; Seh, Z. W. Fundamentals of MXene synthesis. *Nat. Synth.* **2022**, *1*, 601-14. DOI
72. Barsoum, M. W. The $M_{N+1}AX_N$ phases: a new class of solids: thermodynamically stable nanolaminates. *Prog. Solid. State. Chem.* **2000**, *28*, 201-81. DOI
73. Mathis, T. S.; Maleski, K.; Goad, A.; et al. Modified MAX phase synthesis for environmentally stable and highly conductive Ti_3C_2 MXene. *ACS. Nano.* **2021**, *15*, 6420-9. DOI
74. VahidMohammadi, A.; Rosen, J.; Gogotsi, Y. The world of two-dimensional carbides and nitrides (MXenes). *Science* **2021**, *372*, eabf1581. DOI PubMed
75. Khaledialidusti, R.; Khazaei, M.; Khazaei, S.; Ohno, K. High-throughput computational discovery of ternary-layered MAX phases and prediction of their exfoliation for formation of 2D MXenes. *Nanoscale* **2021**, *13*, 7294-307. DOI PubMed
76. Ghidiu, M.; Lukatskaya, M. R.; Zhao, M. Q.; Gogotsi, Y.; Barsoum, M. W. Conductive two-dimensional titanium carbide 'clay' with high volumetric capacitance. *Nature* **2014**, *516*, 78-81. DOI PubMed
77. Li, T.; Yao, L.; Liu, Q.; et al. Fluorine-free synthesis of high-purity $Ti_3C_2T_x$ (T = OH, O) via alkali treatment. *Angew. Chem. Inter. Ed.* **2018**, *57*, 6115-9. DOI
78. Li, M.; Lu, J.; Luo, K.; et al. Element Replacement approach by reaction with lewis acidic molten salts to synthesize nanolaminated MAX phases and MXenes. *J. Am. Chem. Soc.* **2019**, *141*, 4730-7. DOI
79. Li, M.; Li, X.; Qin, G.; et al. Halogenated Ti_3C_2 MXenes with electrochemically active terminals for high-performance zinc ion batteries. *ACS. Nano.* **2021**, *15*, 1077-85. DOI
80. Naguib, M.; Unocic, R. R.; Armstrong, B. L.; Nanda, J. Large-scale delamination of multi-layers transition metal carbides and carbonitrides "MXenes". *Dalton. Trans.* **2015**, *44*, 9353-8. DOI PubMed
81. Naguib, M.; Mochalin, V. N.; Barsoum, M. W.; Gogotsi, Y. 25th anniversary article: MXenes: a new family of two-dimensional materials. *Adv. Mater.* **2014**, *26*, 992-1005. DOI PubMed
82. Alhabeb, M.; Maleski, K.; Anasori, B.; et al. Guidelines for synthesis and processing of two-dimensional titanium carbide ($Ti_3C_2T_x$ MXene). *Chem. Mater.* **2017**, *29*, 7633-44. DOI
83. Maleski, K.; Mochalin, V. N.; Gogotsi, Y. Dispersions of two-dimensional titanium carbide MXene in organic solvents. *Chem. Mater.* **2017**, *29*, 1632-40. DOI
84. Al-Temimy, A.; Anasori, B.; Mazzio, K. A.; et al. Enhancement of Ti_3C_2 MXene pseudocapacitance after urea intercalation studied by soft X-ray absorption spectroscopy. *J. Phys. Chem. C.* **2020**, *124*, 5079-86. DOI
85. Mashtalir, O.; Naguib, M.; Mochalin, V. N.; et al. Intercalation and delamination of layered carbides and carbonitrides. *Nat. Commun.* **2013**, *4*, 1716. DOI
86. Xu, J.; Peng, T.; Zhang, Q.; Zheng, H.; Yu, H.; Shi, S. Intercalation effects on the electrochemical properties of $Ti_3C_2T_x$ MXene nanosheets for high-performance supercapacitors. *ACS. Appl. Nano. Mater.* **2022**, *5*, 8794-803. DOI
87. Li, J.; Yuan, X.; Lin, C.; et al. Achieving high pseudocapacitance of 2D titanium carbide (MXene) by cation intercalation and surface modification. *Adv. Energy. Mater.* **2017**, *7*, 1602725. DOI
88. Lipatov, A.; Alhabeb, M.; Lukatskaya, M. R.; Boson, A.; Gogotsi, Y.; Sinitskii, A. Effect of synthesis on quality, electronic properties and environmental stability of individual monolayer Ti_3C_2 MXene flakes. *Adv. Elect. Mater.* **2016**, *2*, 1600255. DOI
89. Shahzad, F.; Alhabeb, M.; Hatter, C. B.; et al. Electromagnetic interference shielding with 2D transition metal carbides (MXenes). *Science* **2016**, *353*, 1137-40. DOI
90. Greaves, M.; Mende, M.; Wang, J.; Yang, W.; Barg, S. Investigating the rheology of 2D titanium carbide (MXene) dispersions for colloidal processing: progress and challenges. *J. Mater. Res.* **2021**, *36*, 4578-600. DOI
91. Abdolhosseinzadeh, S.; Jiang, X.; Zhang, H.; Qiu, J.; Zhang, C. Perspectives on solution processing of two-dimensional MXenes. *Mater. Today.* **2021**, *48*, 214-40. DOI
92. Uzun, S.; Schelling, M.; Hantanasirisakul, K.; et al. Additive-free aqueous MXene inks for thermal inkjet printing on textiles. *Small* **2021**, *17*, 2006376. DOI
93. Quain, E.; Mathis, T. S.; Kurra, N.; et al. Direct writing of additive-free MXene-in-water ink for electronics and energy storage. *Adv.*

Mater. Technol. **2019**, *4*, 1800256. DOI
94. Robertson, G. L. Food packaging: principles and practice, third edition. CRC press; 2005. p. 733.
95. Hu, G.; Albrow-Owen, T.; Jin, X.; et al. Black phosphorus ink formulation for inkjet printing of optoelectronics and photonics. *Nat. Commun.* **2017**, *8*, 278. DOI PubMed PMC
96. El-Kady, M. F.; Kaner, R. B. Scalable fabrication of high-power graphene micro-supercapacitors for flexible and on-chip energy storage. *Nat. Commun.* **2013**, *4*, 1475. DOI PubMed
97. Beidaghi, M.; Gogotsi, Y. Capacitive energy storage in micro-scale devices: recent advances in design and fabrication of micro-supercapacitors. *Energy. Environ. Sci.* **2014**, *7*, 867. DOI
98. Peng, Y. Y.; Akuzum, B.; Kurra, N.; et al. All-MXene (2D titanium carbide) solid-state microsupercapacitors for on-chip energy storage. *Energy. Environ. Sci.* **2016**, *9*, 2847-54. DOI
99. Kurra, N.; Hota, M. K.; Alshareef, H. N. Conducting polymer micro-supercapacitors for flexible energy storage and Ac line-filtering. *Nano. Energy.* **2015**, *13*, 500-8. DOI
100. Wang, N.; Liu, J.; Zhao, Y.; Hu, M.; Qin, R.; Shan, G. Laser-cutting fabrication of Mxene-based flexible micro-supercapacitors with high areal capacitance. *ChemNanoMat* **2019**, *5*, 658-65. DOI
101. Li, X.; Chen, R.; Zhao, Y.; et al. Layer-by-layer inkjet printing GO film anchored $Ni(OH)_2$ nanoflakes for high-performance supercapacitors. *Chem. Eng. J.* **2019**, *375*, 121988. DOI
102. Ng, L. W. T.; Hu, G.; Howe, R. C. T.; et al. Printing of graphene and related 2D materials: technology, formulation and applications. Cham: Springer International Publishing; 2019. p. 220. DOI
103. Wu, C. W.; Unnikrishnan, B.; Chen, I. W. P.; Harroun, S. G.; Chang, H. T.; Huang, C. C. Excellent oxidation resistive MXene aqueous ink for micro-supercapacitor application. *Energy. Stor. Mater.* **2020**, *25*, 563-71. DOI
104. Wen, D.; Ying, G.; Liu, L.; et al. Direct inkjet printing of flexible MXene/graphene composite films for supercapacitor electrodes. *J. Alloys. Compd.* **2022**, *900*, 163436. DOI
105. Yu, L.; Fan, Z.; Shao, Y.; Tian, Z.; Sun, J.; Liu, Z. Versatile N-doped MXene ink for printed electrochemical energy storage application. *Adv. Energy. Mater.* **2019**, *9*, 1901839. DOI
106. Zhou, G.; Li, M. C.; Liu, C.; Wu, Q.; Mei, C. 3D printed $Ti_3C_2T_x$ MXene/cellulose nanofiber architectures for solid-state supercapacitors: ink rheology, 3D printability, and electrochemical performance. *Adv. Funct. Mater.* **2022**, *32*, 2109593. DOI
107. Yuan, M.; Wang, L.; Liu, X.; et al. 3D printing quasi-solid-state micro-supercapacitors with ultrahigh areal energy density based on high concentration MXene sediment. *Chem. Eng. J.* **2023**, *451*, 138686. DOI
108. Wen, D.; Ying, G.; Liu, L.; et al. Flexible and high-performance MXene/MnO_2 film electrodes fabricated by inkjet printing: toward a new generation supercapacitive application. *Adv. Mater. Inter.* **2021**, *8*, 2101453. DOI
109. Sun, P.; Liu, J.; Liu, Q.; et al. An inkjet-printing ink based on porous NiS/N-MXene for high-performance asymmetric micro-supercapacitors and self-powered microelectronics. *Chem. Eng. J.* **2023**, *474*, 145466. DOI
110. Sangili, A.; Unnikrishnan, B.; Nain, A.; et al. Stable carbon encapsulated titanium carbide MXene aqueous ink for fabricating high-performance supercapacitors. *Energy. Stor. Mater.* **2022**, *53*, 51-61. DOI
111. Orangi, J.; Hamade, F.; Davis, V. A.; Beidaghi, M. 3D printing of additive-free 2D $Ti_3C_2T_x$ (MXene) ink for fabrication of micro-supercapacitors with ultra-high energy densities. *ACS. Nano.* **2019**, *14*, 640-50. DOI
112. Zhao, J.; Lu, H.; Wei, X.; Gao, Y.; Song, Y.; Xu, B. Direct writing additive-free V_2CT_x MXene architectures enables Zn-ion hybrid capacitor with ultrahigh energy density. *J. Energy. Stor.* **2023**, *66*, 107481. DOI
113. Wen, D.; Wang, X.; Liu, L.; et al. Inkjet printing transparent and conductive MXene ($Ti_3C_2T_x$) films: a strategy for flexible energy storage devices. *ACS. Appl. Mater. Interfaces.* **2021**, *13*, 17766-80. DOI
114. Alam, A.; Saeed, G.; Kim, K. W.; Kim, J. K.; Park, H. S.; Lim, S. Direct ink writing (DIW) printed high-performance asymmetric supercapacitor based on 0D@2D silver-nanoparticles@MXene as anode and 0D@2D MnO_2-nanoparticles@MXene as cathode materials. *J. Energy. Stor.* **2023**, *72*, 108227. DOI
115. Abdolhosseinzadeh, S.; Heier, J.; Zhang, C. Coating porous MXene films with tunable porosity for high-performance solid-state supercapacitors. *ChemElectroChem* **2021**, *8*, 1911-7. DOI
116. Zhang, S.; Huang, Y.; Ruan, Y.; Wang, J.; Han, X.; Sun, X. Electrostatic self-assembly of citrus based carbon nanosheets and MXene: flexible film electrodes and patterned interdigital electrodes for all-solid supercapacitors. *J. Energy. Stor.* **2023**, *58*, 106392. DOI
117. Li, L.; Zhang, N.; Zhang, M.; Zhang, X.; Zhang, Z. Flexible $Ti_3C_2T_x$/PEDOT:PSS films with outstanding volumetric capacitance for asymmetric supercapacitors. *Dalton. Trans.* **2019**, *48*, 1747-56. DOI
118. Wang, Y.; Zhang, Y. Z.; Dubbink, D.; ten Elshof, J. E. Inkjet printing of δ-MnO_2 nanosheets for flexible solid-state micro-supercapacitor. *Nano. Energy.* **2018**, *49*, 481-8. DOI
119. McManus, D.; Vranic, S.; Withers, F.; et al. Water-based and biocompatible 2D crystal inks for all-inkjet-printed heterostructures. *Nat. Nanotechnol.* **2017**, *12*, 343-50. DOI
120. Torrisi, F.; Hasan, T.; Wu, W.; et al. Inkjet-printed graphene electronics. *ACS. Nano.* **2012**, *6*, 2992-3006. DOI
121. Pereira, N. M.; Rezende, N. P.; Cunha, T. H. R.; et al. Aerosol-printed MoS_2 ink as a high sensitivity humidity sensor. *ACS. Omega.* **2022**, *7*, 9388-96. DOI PubMed PMC
122. Carey, T.; Cacovich, S.; Divitini, G.; et al. Fully inkjet-printed two-dimensional material field-effect heterojunctions for wearable and textile electronics. *Nat. Commun.* **2017**, *8*, 1202. DOI PubMed PMC

123. Reis, N.; Derby, B. Ink jet deposition of ceramic suspensions: modeling and experiments of droplet formation. *MRS. Proc.* **2000**, *625*, S1946427400193224. DOI
124. Ma, J.; Zheng, S.; Cao, Y.; et al. Aqueous MXene/PH1000 hybrid inks for inkjet-printing micro-supercapacitors with unprecedented volumetric capacitance and modular self-powered microelectronics. *Adv. Energy. Mater.* **2021**, *11*, 2100746. DOI
125. Zhang, C. J.; Pinilla, S.; McEvoy, N.; et al. Oxidation stability of colloidal two-dimensional titanium carbides (MXenes). *Chem. Mater.* **2017**, *29*, 4848-56. DOI
126. Ataide, V. N.; Mendes, L. F.; Gama, L. I. L. M.; de, A. W. R.; Paixão, T. R. L. C. Electrochemical paper-based analytical devices: ten years of development. *Anal. Methods.* **2020**, *12*, 1030-54. DOI
127. Somalu, M. R.; Muchtar, A.; Daud, W. R. W.; Brandon, N. P. Screen-printing inks for the fabrication of solid oxide fuel cell films: a review. *Renew. Sustain. Energy. Rev.* **2017**, *75*, 426-39. DOI
128. Abdolhosseinzadeh, S.; Schneider, R.; Verma, A.; Heier, J.; Nüesch, F.; Zhang, C. J. Turning trash into treasure: additive free MXene sediment inks for screen-printed micro-supercapacitors. *Adv. Mater.* **2020**, *32*, e2000716. DOI PubMed
129. Hussain, I.; Lamiel, C.; Javed, M. S.; et al. MXene-based heterostructures: current trend and development in electrochemical energy storage devices. *Progr. Energy. Combust. Sci.* **2023**, *97*, 101097. DOI
130. Li, H.; Li, X.; Liang, J.; Chen, Y. Hydrous RuO_2-decorated MXene coordinating with silver nanowire inks enabling fully printed micro-supercapacitors with extraordinary volumetric performance. *Adv. Energy. Mater.* **2019**, *9*, 1803987. DOI
131. Carlson, A.; Bowen, A. M.; Huang, Y.; Nuzzo, R. G.; Rogers, J. A. Transfer printing techniques for materials assembly and micro/nanodevice fabrication. *Adv. Mater.* **2012**, *24*, 5284-318. DOI PubMed
132. Xu, B.; Zhu, M.; Zhang, W.; et al. Ultrathin MXene-micropattern-based field-effect transistor for probing neural activity. *Adv. Mater.* **2016**, *28*, 3333-9. DOI
133. Zhang, Y.; Shi, G.; Qin, J.; et al. Recent progress of direct ink writing of electronic components for advanced wearable devices. *ACS. Appl. Electron. Mater.* **2019**, *1*, 1718-34. DOI
134. Yang, W.; Yang, J.; Byun, J. J.; et al. 3D printing of freestanding MXene architectures for current-collector-free supercapacitors. *Adv. Mater.* **2019**, *31*, e1902725. DOI
135. Li, X.; Li, H.; Fan, X.; Shi, X.; Liang, J. 3D-printed stretchable micro-supercapacitor with remarkable areal performance. *Adv. Energy. Mater.* **2020**, *10*, 1903794. DOI
136. Wang, J.; Ma, X.; Zhou, J.; Du, F.; Teng, C. Bioinspired, high-strength, and flexible MXene/aramid fiber for electromagnetic interference shielding papers with joule heating performance. *ACS. Nano.* **2022**, *16*, 6700-11. DOI PubMed
137. Zhou, B.; Su, M.; Yang, D.; et al. Flexible MXene/silver nanowire-based transparent conductive film with electromagnetic interference shielding and electro-photo-thermal performance. *ACS. Appl. Mater. Interfaces.* **2020**, *12*, 40859-69. DOI
138. Ma, Z.; Kang, S.; Ma, J.; et al. Ultraflexible and mechanically strong double-layered aramid nanofiber- $Ti_3C_2T_x$ MXene/silver nanowire nanocomposite papers for high-performance electromagnetic interference shielding. *ACS. Nano.* **2020**, *14*, 8368-82. DOI
139. Xie, Y.; Zhang, H.; Huang, H.; et al. High-voltage asymmetric MXene-based on-chip micro-supercapacitors. *Nano. Energy.* **2020**, *74*, 104928. DOI
140. Patil, G. C. Doctor blade: a promising technique for thin film coating. Singapore: Springer; 2023. pp. 509-30. DOI
141. Guo, T.; Zhou, D.; Deng, S.; et al. Rational design of $Ti_3C_2T_x$ MXene inks for conductive, transparent films. *ACS. Nano.* **2023**, *17*, 3737-49. DOI
142. Guo, T.; Zhou, D.; Gao, M.; et al. Large-area smooth conductive films enabled by scalable slot-die coating of $Ti_3C_2T_x$ MXene aqueous inks. *Adv. Funct. Mater.* **2023**, *33*, 2213183. DOI
143. Huang, X.; Wu, P. A facile, high-yield, and freeze-and-thaw-assisted approach to fabricate MXene with plentiful wrinkles and its application in on-chip micro-supercapacitors. *Adv. Funct. Mater.* **2020**, *30*, 1910048. DOI
144. Lucero, N.; Vilcarino, D.; Datta, D.; Zhao, M. Q. The roles of MXenes in developing advanced lithium metal anodes. *J. Energy. Chem.* **2022**, *69*, 132-49. DOI
145. Zheng, J.; Kim, M. S.; Tu, Z.; Choudhury, S.; Tang, T.; Archer, L. A. Regulating electrodeposition morphology of lithium: towards commercially relevant secondary Li metal batteries. *Chem. Soc. Rev.* **2020**, *49*, 2701-50. DOI PubMed
146. Fan, X.; Chen, L.; Borodin, O.; et al. Non-flammable electrolyte enables Li-metal batteries with aggressive cathode chemistries. *Nat. Nanotechnol.* **2018**, *13*, 715-22. DOI
147. Shen, K.; Li, B.; Yang, S. 3D printing dendrite-free lithium anodes based on the nucleated MXene arrays. *Energy. Stor. Mater.* **2020**, *24*, 670-5. DOI
148. Chen, Q.; Wei, Y.; Zhang, X.; et al. Vertically aligned MXene nanosheet arrays for high-rate lithium metal anodes. *Adv. Energy. Mater.* **2022**, *12*, 2200072. DOI
149. Ma, J.; Zheng, S.; Zhou, F.; et al. All 3D printing lithium metal batteries with hierarchically and conductively porous skeleton for ultrahigh areal energy density. *Energy. Stor. Mater.* **2023**, *54*, 304-12. DOI
150. Zhang, X.; Kong, D.; Li, X.; Zhi, L. Dimensionally designed carbon-silicon hybrids for lithium storage. *Adv. Funct. Mater.* **2019**, *29*, 1806061. DOI
151. Chae, S.; Choi, S. H.; Kim, N.; Sung, J.; Cho, J. Integration of graphite and silicon anodes for the commercialization of high-energy lithium-ion batteries. *Angew. Chem. Int. Ed.* **2020**, *59*, 110-35. DOI
152. Zhang, C. J.; Park, S. H.; Seral-Ascaso, A.; et al. High capacity silicon anodes enabled by MXene viscous aqueous ink. *Nat. Commun.* **2019**, *10*, 849. DOI PubMed PMC

153. Pang, Q.; Liang, X.; Kwok, C. Y.; Nazar, L. F. Advances in lithium-sulfur batteries based on multifunctional cathodes and electrolytes. *Nat. Energy.* **2016**, *1*, 1-11. DOI
154. Tang, H.; Li, W.; Pan, L.; et al. In situ formed protective barrier enabled by sulfur@titanium carbide (MXene) ink for achieving high-capacity, long lifetime Li-S batteries. *Adv. Sci.* **2018**, *5*, 1800502. DOI PubMed PMC
155. Wei, C.; Tian, M.; Fan, Z.; et al. Concurrent realization of dendrite-free anode and high-loading cathode via 3D printed N-Ti_3C_2 MXene framework toward advanced Li-S full batteries. *Energy. Stor. Mater.* **2021**, *41*, 141-51. DOI
156. Wang, Y.; Lubbers, T.; Xia, R.; et al. Printable two-dimensional V_2O_5/MXene heterostructure cathode for lithium-ion battery. *J. Electrochem. Soc.* **2021**, *168*, 020507. DOI
157. Zhang, C.; Zhao, W.; Park, S. H.; et al. Interconnected metallic membrane enabled by MXene inks toward high-rate anode and high-voltage cathode for Li-ion batteries. *Adv. Funct. Mater.* **2023**, *33*, 2213860. DOI
158. Chen, D.; Long, Y.; Wu, Z.; et al. A gelation-assisted approach for versatile MXene inks. *Adv. Funct. Mater.* **2022**, *32*, 2204372. DOI
159. Park, J. M.; Jana, M.; Baek, S. H.; et al. MXene ink hosting zinc anode for high performance aqueous zinc metal batteries. *J. Energy. Chem.* **2023**, *76*, 187-94. DOI
160. Wang, Z.; Huang, Z.; Wang, H.; et al. 3D-printed sodiophilic V_2CT_x/rGO-CNT MXene microgrid aerogel for stable Na metal anode with high areal capacity. *ACS. Nano.* **2022**, *16*, 9105-16. DOI
161. Zheng, J.; Diao, J.; Jin, Y.; et al. An inkjet printed Ti_3C_2-GO electrode for the electrochemical sensing of hydrogen peroxide. *J. Electrochem. Soc.* **2018**, *165*, B227-31. DOI
162. Su, Y.; Liu, B.; Zhang, Q.; et al. Printing-scalable $Ti_3C_2T_x$ MXene-decorated janus separator with expedited Zn^{2+} flux toward stabilized Zn anodes. *Adv. Funct. Mater.* **2022**, *32*, 2204306. DOI